A

DISSERTATION REPORT

ON

INVESTIGATION ON METAL-INSULATOR-METAL (MIM) BASED PLASMONIC GRATING FOR BAND STOP FILTERING

is submitted as a partial fulfillment of the degree of

MASTER OF TECHNOLOGY

in

ELECTRONICS AND COMMUNICATON

to the

DEPARTMENT OF ELECTRONICS AND COMMUNICATION ENGINEERING

by

HARDIK MATHURIYA

(2017PEC5114)

Under the guidance of

Dr. GHANSHYAM SINGH

Electronics & Communication Engineering Department

Malaviya National Institute of Technology, Jaipur

JULY 2019

DEPARTMENT OF ELECTRONICS & COMMUNICATION ENGINEERING
MALAVIYA NATIONAL INSTITUTE OF TECHNOLOGY
JAIPUR (RAJASTHAN) – 302017

Certificate

This is to certify that the dissertation report entitled **Investigation on Metal-Insulator-Metal (MIM) based Plasmonic Grating for band stop filtering** submitted by **Hardik Mathuriya (2017PEC5114)**, in the partial fulfilment of the Degree Master of Technology in **Electronics and Communication** of Malaviya National Institute of Technology, is the work completed by him under our supervision, and approved for submission during academic session 2018-2019.

Dr. Ghanshyam Singh
(Project Supervisor)
Professor
Dept. of ECE
MNIT Jaipur

Date:

Place:

DEPARTMENT OF ELECTRONICS & COMMUNICATION ENGINEERING
MALAVIYA NATIONAL INSTITUTE OF TECHNOLOGY
JAIPUR (RAJASTHAN) – 302017

Declaration

I declare that,

a) The work contained in this dissertation is original and has been done by me under the guidance of my supervisor.
b) The work has not been submitted to any other institute for any degree or diploma.
c) I have followed the guidelines provided by the institute in preparing the dissertation.
d) I have confirmed to the norms and guidelines given in the Ethical code of conduct of the institute.
e) Whenever I have used materials (data, theoretical analysis, figures and text from other sources. I have given due credit to them by citing them in the text of the dissertation and giving their details in the references. Further, I have taken permission from the copyright owners of the sources, whenever necessary.

Hardik Mathuriya
M.Tech
Electronics and Communication
Dept. of ECE
2017PEC5114

Date:

Place:

Acknowledgment

*I take immense pleasure in thanking of gratitude to my project supervisor **Dr. Ghanshyam Singh**, Professor, Malaviya National Institute of Technology (MNIT) Jaipur for being a source of inspiration and for timely guidance during the project. The supervision and support that he gave truly helped in the progression of my thesis. I am highly obliged to him for his valuable advices on research and moral support during research period. I am highly thankful to him for his genuine efforts he put in bolstering my career.*

*I express my sincere gratitude to **Prof. D. Boolchandani** (Head of Department) for his support and guidance in this research work. Many thanks to committee members Dr. Vijay Janyani (Professor), Dr. Ritu Sharma (Associate Professor), Dr. M. Ravi Kumar (Assistant Professor), and Dr. Ashish Kumar Ghunawat (Assistant Professor) for their valuable comments and guidance in research exploration, without this guidance it was not possible to achieve these good results in this research work. I would like to thank Dr. Sourabh Sahu for his priceless guidance. I would also like to thank Mr. Vijay Singh and Mr. Deepak for allowing me in laboratories over time.*

*I would like to express my special appreciation and thanks to **Dr. Rukhsar Zafar,** Swami Keshvanand Institute of Technology, Management and Gramothan (SKIT), Jaipur for guiding me with her immense knowledge and research experience. Her advice on both research and my career have been invaluable. She has been a true inspiration for me. I thank her from the bottom of my heart for her unconditional mentoring.*

A special thanks to my family. Words cannot express the sacrifices my grandmother, my uncle and my parents have made on my behalf. I would also like to thank my friends who supported me in writing and incented me to strive towards my goal.

I would also like to thank Ministry of HRD, Government of India for its support to me to pursue my Masters in Wireless and Optical Communication Engineering from Malaviya National Institute of Technology, Jaipur. This support provided me library, laboratory, hostel and other related infrastructure.

Hardik Mathuriya

Abstract

The technological advances in the recent era have expanded the range of functionalities for integrated photonic circuits. An emerging branch of Photonics named as Plasmonics pave the way for practical realization of the fantasy of optical integrated circuits. Plasmonics provides a key solution to provide sub-wavelength confinement and lends a hand in designing photonic integrated circuits. Plasmonics deals with the basic phenomenon of Electromagnetic (EM) interaction with metals.

Metal-Insulator-Metal (MIM) waveguide supports a unique feature of deep sub-wavelength confinement and overcomes the diffraction limit of light. The appealing feature of confining signal at sub-wavelength scale in MIM waveguide offers ultra small foot-print. In this work, MIM based Plasmonic grating has been numerically investigated for band stop filtering. This is designed by periodic arrangement of stub resonators keeping the separation between adjacent resonators same in the MIM structure. This grating exhibits nice filtering characteristics. The proposed device offers a stop band near 1550 nm wavelength since most of the optical devices or networks are designed to operate in this desired band due to low loss and attenuation.

Special mode or defect mode is excited in stop band by introducing a defect state (region) in the perfect plasmonic MIM grating. The defect region is created in waveguide grating and a metallic slit is placed in the centre position of the defect region. In the presence of metallic slit, resonance splitting is observed due to interaction of dark and bright resonance modes. This resonance splitting is generally emerged due to Fano resonance phenomena. Fano principle based resonance provides an increased value of quality factor as compared to traditional resonance.

The proposed device is also explored for switching purpose. By filling a non-linear material into the defect region and exciting Fano resonance in the grating, multiple switching at different wavelengths is observed. The performance of device is quantified using modulation depth. Finally, the refractive index sensing property of the device is also explored. This Plasmonic grating is viable for designing optical de-multiplexers, sensors, filters etc.

List of Abbreviations

SPR	-	Surface Plasmon Resonance
MIM	-	Metal-Insulator-Metal
MDM	-	Metal-Dielectric-Metal
SPP	-	Surface Plasmon Polariton
SPP-WBG	-	Surface Plasmon Polariton Waveguide Bragg Grating
FOM	-	Figure of Merit
THz	-	Terahertz
PIT	-	Plasmon-Induced Transparency
EOT	-	Extra-Ordinary Transmission
TEM	-	Transverse Electromagnetic
TE	-	Transverse Electric
TM	-	Transverse Magnetic
TIR	-	Total Internal Reflection
NA	-	Numerical Aperture
GSPP	-	Coupled Gap Surface Plasmon Polariton
IMI	-	Insulator-Metal-Insulator
FDTD	-	Finite Difference Time Domain
PML	-	Perfectly Matched Layer
FBG	-	Fibre Bragg Grating
FWHM	-	Full Width at Half Maximum
MD	-	Modulation Depth
RI	-	Refractive Index

List of Symbols

nm	-	Nanometer
δ_d	-	Skin Depth in Dielectric
δ_m	-	Skin Depth in Metal
ε_m	-	Relative permittivity of Metal
Ω_p	-	Plasma Frequency
n	-	Free Electron Density
ε_o	-	Free Space Permeability
m	-	Effective mass of free electron
e	-	Electronic Charge
Υ	-	Collision Frequency
k_z	-	Propagation Constant
κ	-	Inverse Penetration Depth
c	-	Speed of Light
Ω_{SPP}	-	Resonant Frequency of Surface Plasmon Polariton
θ	-	Incident Angle
k_o	-	Free Space Propagation Constant
G	-	Grating Reciprocal Vector
a	-	Lattice Constant
ε_d	-	Relative Permittivity of Dielectric
k_{G-SPP}	-	Propagation Constant of GSPP
µm	-	Micrometer
λ	-	Wavelength
N	-	Period Number
L_1	-	Resonator length
L_2	-	Insulator length
W_1	-	Resonator Width
W_2	-	Insulator Width

L_3	-	Defect length
Q	-	Quality Factor
t	-	Slit Width
α	-	Transverse Wave-Vector
Δx	-	Step Size in x-direction
Δz	-	Step Size in z-direction
Δd	-	Shift in the position of slit
E	-	Electric Field
T	-	Transmission Efficiency
S	-	Sensitivity
esu	-	Electrostatic Unit

Table of Contents

List of Figures

List of Tables

1. INTRODUCTION

1.1. Technological developments

The gradual growth of human society and technology has led to an escalating demand of miniaturizing electronic circuits and devices. Moore's law governing the semiconductor industry for over 50 years asserts that the transistor count on a silicon chip doubles every 18 months leading to highly computationally powerful processors. The scaling of transistors results in enhanced performance with the downside of excessive heat generation detrimental to whole chip. This stands as an impediment to the fulfilment of high speed data processing [1-2]. Furthermore, there is an economic aspect putting an end to Moore's law [3].

A promising solution to the above problem is the use of optical signals. The speed of light in a semiconductor material is much greater than speed of electrons. Furthermore, optical signal is less prone to energy losses making it suitable for carrying information at higher data rates. This has promoted the proliferation of photonic circuits [4]. Photonic crystal structures provide faster processing speeds, improved bandwidth and greater immunity to electromagnetic interference compared with electronic circuits [4-9]. However, the diffraction limit of light restricts the flow of optical energy inside photonic devices and limiting their miniaturization towards sub-wavelength scale [10-11]. The size of photonic devices is typically half a wavelength of light making them considerably bigger than their electronic counterparts. This pronounced mismatching of size between photonic and electronic devices poses a serious challenge for their interfacing [12]. An emerging device technology known as Plasmonics provides a fascinating way to overcome the size mismatch problem. It facilitates information flow between nanoscale devices and helps in bridging the gap between electronic and optical domains [14-16].

Plasmonics, a field of Nanophotonics has emerged, aimed at overcoming the diffraction limit of light and producing deep subwavelength photonic devices. Plasmonics pertains to the interaction of conduction electrons with electromagnetic energy at metal-dielectric interfaces. It examines the confinement of electromagnetic waves in the sub-100-nm dimension way beyond diffraction limit [14]. This intriguing feature has made possible the creation of nanoscale photonic infrastructure for applications in biological

sensing [17], slow light generation [18], switching [19], de-multiplexing [20-21] and so on.

1.2. Motivation

The demand of high speed data processing has been steadily increasing over the last decades. The minimization of electronic circuits has become essential to fulfil the urgent need of high speed. The problem associated with the miniaturization of the devices is that the delay of electronic circuits also increases which serves as a hindrance to the data transportation capabilities.

Since the drift velocity of the electrons is not large the electronic interconnects lack the enormous speed for information processing. This can be accomplished by their optical counterpart i.e. optical fibre cables. The drawback of using optical fibres cables over electronic circuits is that they are thousand times heavier. This has laid the foundation for the development of optical circuits.

Plasmonics aims to miniaturize the optical circuits at the level of the electronic circuits and to overcome the diffraction limit. It combines the merits of photonics (large bandwidths) with electronics (nanoscale miniaturization). Surface Plasmon Resonance (SPR) the base of Plasmonics, has become one of the widely used optical techniques owing to its appealing characteristic of on-chip integration of photonic circuits.

An on-chip optical filter is an important and appealing research field in the area of Nanophotonics. In addition to this, Plasmonics finds applications in the fields of on-chip optical buffering [22], biological sensing [23], narrow band filtering [], refractive index sensing [24] etc.

1.3. Research Contribution

In this proposed research work, metal-insulator-metal (MIM) or metal-dielectric-metal (MDM) based Plasmonic grating has been designed to achieve band stop filtering characteristics. Several variants of Plasmonic grating have been designed and numerically investigated and a comprehensive analysis of their transmission characteristics and their dependence on geometrical parameters is successfully carried out. In the transmission spectrum, a minute transmission window is induced in the stop band. This transmission window termed as defect mode arises by introducing a defect length in the perfect Plasmonic structure. This defect mode produced in the grating makes it suitable for sensing, filtering and demultiplexing based applications.

A metallic nano-slit is introduced in this defect region by virtue of which a resonance exhibiting an asymmetrical profile called as Fano resonance is excited in the MIM waveguide based grating. The analysis of this Fano resonance excited grating for multiple switching applications is carried out. Furthermore, the sensing based applications of Plasmonic grating is also thoroughly explored by exciting Fano resonance.

1.4. Thesis Organization

The thesis contains five chapters with the following arrangement:

Chapter 2 covers the earlier work in the field of Plasmonics pertaining to filtering.

Chapter 3 has been dedicated to the comprehensive analysis of Surface Plasmon Polaritons (SPPs). The fundamentals of the SPP propagation and the excitation methods are discussed in detail. The modelling of the metal permittivity and types of metal-insulator-metal waveguides are explained.

Chapter 4 is related to the designing and analysis of different MIM based Plasmonic gratings and their applications in switching and refractive index sensing.

Chapter 5 summarizes the work and deals with future aspects.

2. LITERATURE REVIEW

Zhanghua Han et al. [25] proposed and numerically simulated a surface plasmon polariton Bragg grating labelled as SPP-WBG. This SPP-WBG is formed by periodically modulating the insulator width in a MIM waveguide. This waveguide structure exhibits good band stop filtering characteristics. In the transmission spectrum, the ripples obtained are suppressed by using S-shaped Bragg cells and performance is improved. A defect region is introduced into the SPP-WBG by virtue of which a small transmission window in the stop band is obtained which results in high quality factor.

Feifei Hu et al. [26] proposed a sub-wavelength surface plasmon band pass filter based on two MIM waveguides and a slot cavity. By shifting the input and output waveguides the pass band is selected and the light can be spectrally split. The modulation of the cavity parameters and the coupling distance results in bandwidth adjustment. The results indicate that this ultra-compact sensor is suitable for applications in integrated photonic circuits on metal surfaces.

Gaige Zheng et al. [27] designed a tunable MIM circular ring resonator based band-pass filter. A non-linear Kerr material is filled into the ring resonator. By varying the intensity of light the transmitted peak can be easily tuned. At the desired wavelength, narrow band filtering is easily achieved by varying the intensity of light as it governs the resonance wavelength tuning.

Xi Chen et al. [28] presented nanoscale structures based on MIM waveguides and two nano ring resonators. The change in the coupling mode between the resonators and the waveguides yield band pass and band stop filtering characteristics. With the increase in the resonator size the characteristic wavelength of the filters increases. The double ring resonator based filters indicate higher sensitivity on wavelength.

Rukhsar Zafar et al. [29] proposed an ultra-compact surface plasmon sensor based on MIM waveguide. The MIM waveguide is paired with two stub resonators and a metallic nano slit of silver is embedded into the stub resonators. The material to be sensed is filled in both MIM waveguide and the stub resonators. By breaking the symmetry in the structure, Fano resonance is excited. The sensor presents very large sensitivity and a high value of Figure of merit (FOM).

Shubin Yen et al. [30] proposed a refractive index sensor made up of two MIM waveguides and a ring resonator. Each waveguide has one sealed end and other ends act as ports. The transmission spectrum exhibits an asymmetric line shape and indicate nice filtering characteristics. The quality factor quantifies the performance of the filter which increases in linearly with the radius of the resonator. The Fano resonance shows large sensitivity as compared to Lorentzian resonance.

Rukhsar Zafar et al. [31] proposed a metal-dielectric-metal based surface plasmon sensor coupled to stub resonator pair. The separation between resonators is carefully handled so that Fano resonance is excited. The liquid or gaseous material to be sensed is filled in the stub resonators. The sensitivity is analysed as a function of group delay and a high value of phase sensitivity is obtained for per unit refractive index change. There is a linear dependence of phase sensitivity on group delay.

Shinian Qu et al. [32] developed a Bragg grating reflector based on MIM waveguide having a defect. A broad stop band is found in the transmission spectrum. The defect window in the spectrum and the central wavelength is tuned by tailoring the structural parameters.

Zhongchao Wei et al. [33] proposed a plasmonic band-stop filter using single and double layered graphene metamaterial in the THz regime. Two graphene ribbons constitute the metamaterial unit cell. By varying the doping concentration of these ribbons the shifting in the resonance wavelength is achieved. Symmetry single graphene layer metamaterial can be employed in refractive index sensing due to its high sensitivity whereas asymmetry double graphene layer can be used as a two-circuit switch.

Xin Luo et al. [34] proposed an ultra-compact MIM Bragg grating coupled with a rectangular air cavity. A plasmon-induced transparency (PIT) response is proposed in the device. The dependence of transmission on air cavity thickness and on the coupling distance between insulator and the cavity is studied.

Rukhsar Zafar et al. [35] investigated a sub-wavelength plasmonics sensor excited by Fano resonance. The interaction between MIM waveguides and two elliptical resonators excite Fano resonance mode. Due to this asymmetric Fano resonance, the proposed plasmonics sensor exhibits large values of sensitivity and FOM. By modifying the

geometrical parameters, the sensing performance can be highly enhanced. The device is tested for haemoglobin detection in blood.

Tahir Iqbal et al. [36] investigated the dependence of surface plasmon resonance as well as plasmonic band gap on the structural parameters of 1 D nanograting. Different nanograting structures are modelled as gold films on glass substrate. The bandgap energy increases with the slit width and starts decreasing when the width of slit equals half the periodicity. As long as the gold depth and the film thickness are comparable the bandgap energy is directly proportional to the film thickness.

3. ANALYSIS OF SURFACE PLASMON POLARITONS

3.1.Introduction

Plasmons and Photons are the fundamental excitations in a material exhibiting conducting properties such as metal or extremely doped semiconductors. The free electron model considers metals as a gas of free electrons that are allowed to move freely within them [14, 37]. These electrons participate in electrical conduction and move independently throughout the lattice without interacting with each other and with the ion cores. Thus, the free electrons form the metal plasma comprising of positively charged ions and negatively charged electrons. Due to the low mass of electrons they possess higher kinetic energies than those of ions. As a result of which the coupled excitation of electrons i.e. plasmons completely dominate the collective excitations of ions i.e. phonons [14,38]. This work is carried out considering only the influence of plasmons. Plasmon is a quantum of collective excitation of conduction electrons inside a conducting media [14]. There are two types of plasmons namely, Volume plasmon and Surface plasmon. Volume plasmons or Bulk plasmons arise due to longitudinal oscillations of electrons in a bulk material, whereas Surface plasmon is described as a surface wave arising by virtue of oscillations of free electron density at conductor surface [14]. Surface plasmons can be excited by electrons as well as photons falling in the visible spectrum. Bulk plasmons can only be excited with an electron beam. The coupling of electrons or photons with the electron plasma generate Surface Plasmon Polariton (SPP). SPP is an electromagnetic surface wave propagating in the parallel direction of the conductor-dielectric interface and is confined perpendicularly [14,38,39].

3.2.History

The history of Plasmonics goes back to fifth century AD when a masterpiece of Romans demonstrating the greatest example of nanotechnology was unveiled to the world. The Lycurgus cup, presently a part of British Museum, London possesses a unique property due to the presence of nanoparticles [40]. When illuminated from behind it shows red colour but when light is passed through it from front green colour appears [38]. Later, Michael Faraday, in 1857 noticed a similar behaviour in metal colloids and observed an eminent change in colour when there was a change in particle size [41-42]. In 1998, the

experiment of Extra-Ordinary Transmission (EOT) redefined the fundamentals on Plasmonics [43]. It demonstrated that when the light is passed through a film of metal patterned with nano-scaled holes, its transmission gets greatly enhanced. This transmission was significantly more than could normally be allowed by nanoscale area. The EOT transmission enlightened an important concept to overcome the diffraction limit i.e. an optical or electromagnetic field can be confined in deep sub-wavelength structures [44]. Furthermore, the growing techniques in the fields of nano-fabrication and nano-lithography [45] have facilitated the realization of nano-scale structures and helped in establishing Plasmonics a major field of research.

3.3.Surface Plasmon Polaritons

Polariton defines a hybrid wave with energy contributed by two sources, the first source is the pure electromagnetic energy accumulated in the electric and magnetic fields and the other source is the energy of solid state. So as the name suggests, SPP is an EM wave that propagates along the interface between a noble metallic portion and dielectric. These waves originate by virtue of the interaction of the incident electromagnetic fields with the oscillations of electron plasma in the metal [15,39,46]. Therefore, the energy of the resulting wave of SPP is contributed by electromagnetic energy and by kinetic energy of free electrons. Fig. 3.1 depicts the excitation of free electrons by EM wave. SPP gets trapped and propagates in the x direction parallel to the metal-dielectric interface. SPP decays evanescently in z direction (both positive and negative) in both the media and eventually dies out after travelling some distance as shown in Fig. 3.2. Skin depth is defined as the distance travelled by this surface wave after which its strength becomes 1/e times of its maximum value and is denoted by δ_d and δ_m in dielectric and metal respectively.

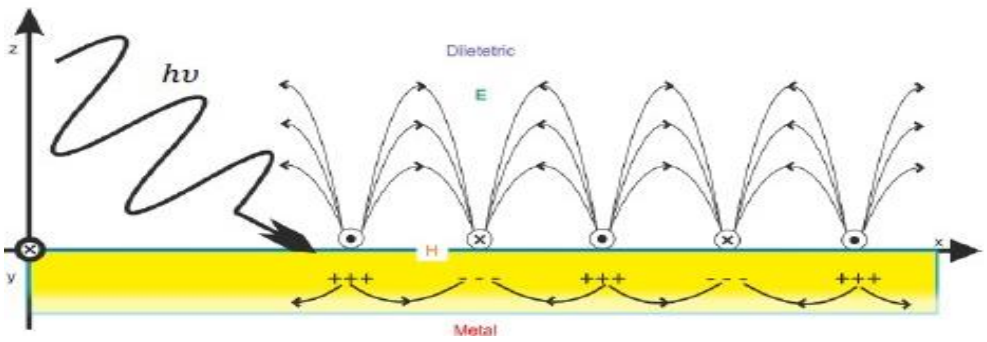

Figure 3.1: Propagation of SPP in the x-direction along the metal-dielectric interface as reported in [46]

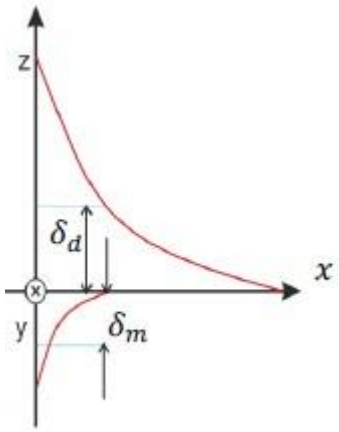

Figure 3.2: Evanescent field of the SPP wave as reported in [46]

By obtaining the general solution of Maxwell's equation in both media it is concluded that surface plasmon modes do not exist for TEM (Transverse Electromagnetic) or TE (Transverse Electric) polarized light but exist only for TM (Transverse Magnetic) polarization of light [14,39]. SPPs can only propagate alongside the interface of those materials whose dielectric constants are of opposite sign [14,39]. Metals exhibit negative dielectric constant in the ultra-high frequency region, while in low-frequency regime they show large conductivity [14]. Electron gas model describes this frequency dependence of valence electrons in a metal [37]. Up to the low frequency part of the spectrum i.e. up to visible region metals possess high reflection characteristics. Electromagnetic fields are restricted to propagate through them. Therefore, the inherent characteristic of infinite conductivity of a perfect conductor is displayed by metals in low frequency regime. As we move towards higher frequencies (infrared and visible region) the fields start penetrating the metals significantly. Finally, metals represent dielectric behaviour at ultraviolet frequencies and thus electromagnetic signal propagates through them with varying levels of attenuation depending on metallic band structures. Alkali metals show transparency while noble metals like silver and gold exhibit strong absorption in ultraviolet regime. The interaction of metal with electromagnetic energy at different frequencies is explained by Drude theory in the next section [39].

3.4.Drude Model

Paul Drude in 1900 proposed the Drude Model to explain the electromagnetic behaviour of electrons. He applied kinetic theory to conduction electrons in metals. His theory is based on following assumptions [14]:

i. Between collisions, the effects of electron-electron and electron-ion interactions are neglected. When no external field is applied electrons move in a straight line between collisions. While in the presence of applied field their motion is governed by Newton's law of motion.

ii. The time elapsed between collisions is τ. The time τ is also known as mean free time or relaxation time. An electron experiences a collision with 1/τ probability per unit time.

iii. Thermal equilibrium is attained by electrons after undergoing collisions with lattice. Electron moves in a random direction after collision with a velocity proportional to the temperature of the region where collision occurred.

According to Drude, permittivity of metal is modelled as:

$$\varepsilon_m(\omega) = 1 - \frac{\Omega_p^2}{\omega^2} \tag{3.1}$$

Here, $\Omega_p = \sqrt{\frac{ne^2}{\varepsilon_o m}}$ is the resonance frequency of free electron gas called plasma frequency, n represents the density of free electrons, e denotes the charge on an electron, ε_o is the permittivity of the vacuum and m denotes the effective mass of free electron.

Fig 3.3 depicts the dependence of metal permittivity on the frequency as reported in [39]. The permittivity is negative for frequencies lower than the plasma frequency and for a static case it tends to minus infinity. Negative reflectivity is a characteristic feature of metals and it results in higher reflectivity. Permittivity tends to one for frequencies much higher than the plasma frequency. It results in transparency of the electron gas for EM waves at these higher frequencies. In the vicinity of the plasma frequency the permittivity is almost zero. This region is termed as Epsilon-near-zero and it is an active research area especially in metamaterial applications.

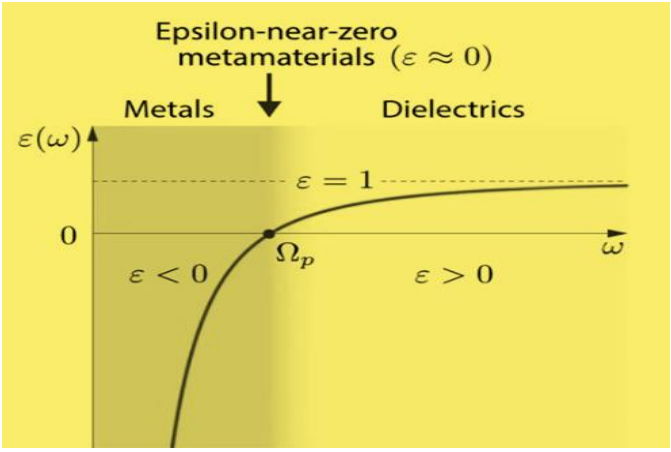

Figure 3.3: Dependence of relative permittivity of metal on frequency as reported in [39]

By taking into account the collisions with defects of the crystal lattice, the Drude formula can be modified as:

$$\varepsilon_m(\omega) = 1 - \frac{\Omega_p^2}{\omega(\omega + i\Upsilon)} \tag{3.2}$$

Here, Υ represents the frequency of collision and is equal to the reciprocal of relaxation time of free electron gas.

Separating the real and imaginary parts of above equation (3.2) we get

$$\varepsilon_m(\omega) = 1 - \frac{\Omega_p^2}{\omega^2 + \Upsilon^2} + i\,\frac{\Upsilon\Omega_p^2}{\omega(\omega^2 + \Upsilon^2)} \tag{3.3}$$

It is clear that both the real and imaginary components and the operating frequency show inverse relation.

To account for the role of bound electrons localized in the vicinity of ions to the dielectric function an offset ε_∞ is appended into equation (3.2) and the equation now becomes

$$\varepsilon_m(\omega) = \varepsilon_\infty - \frac{\Omega_p^2}{\omega(\omega + i\Upsilon)} \tag{3.4}$$

ε_∞ is such a permittivity when concentration of free electrons tends to zero which is the case when plasma frequency becomes zero. The above equation defines the Drude model defining the relative permittivity of the metals.

3.5.SPP analysis at metal/dielectric interface

A single, flat interface is the simplest geometry that can sustain SPPs. As shown in the Fig. 3.4 medium 1 comprises a dielectric that spans the half space (x > 0) exhibiting positive dielectric constant (ε_1) and a conducting medium (metal) having frequency controlled dielectric constant (ε_2) occupies the medium 2 (x < 0).

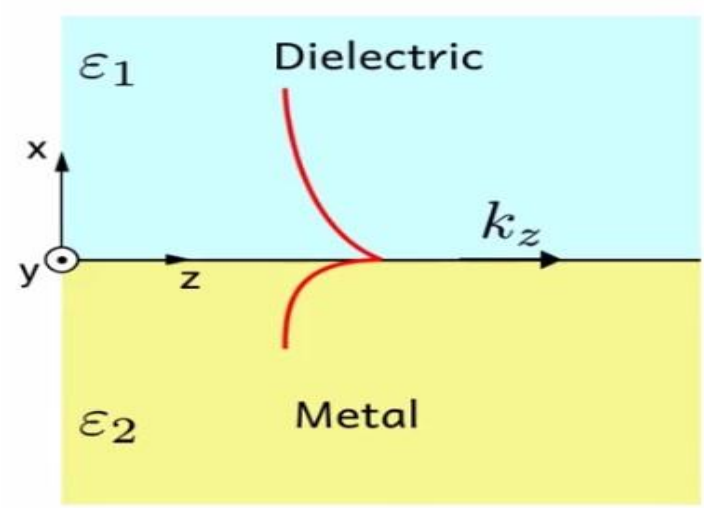

Figure 3.4: SPP at metal/dielectric interface as reported in [39]

It is assumed that the propagation of wave is in the z-direction and the decay is evanescent in the x-direction. The components of the electric and magnetic fields are independent on y-direction. The fields of SPP depend on spatial coordinate in time in the following form

$$E = E(x)e^{-i\omega t + i\,k_z z} \tag{3.5}$$

$$H = H(x)e^{-i\omega t + i\,k_z z} \tag{3.6}$$

The distribution of the fields and the dispersion relation i.e. the dependence of propagation constant k_z on frequency is calculated by cracking the Maxwell's equations in both the media. For TM- polarized light (p-polarized) it is possible to show that in the case of non-magnetic medium non-trivial solutions are obtained. But for TE polarization trivial solutions are obtained. On applying the boundary conditions and maintaining the electric field continuity, following condition is found:

$$\frac{\kappa_1}{\varepsilon_1} + \frac{\kappa_2}{\varepsilon_2} = 0 \tag{3.7}$$

Here, κ_1 and κ_2 are the inverse penetration depths in medium 1 and medium 2 respectively.

$$\kappa_{1,2} = \sqrt{k_z^2 - \varepsilon_{1,2}\,\omega^2/c^2} \tag{3.8}$$

The inverse penetration depths are positive so the solution of the above equation is possible only when one of the dielectric constants ε_1 or ε_2 is negative. After substituting the values of κ_1 and κ_2 in eq. 3.7, it is reduced to

$$\frac{\sqrt{k_z^2 - \varepsilon_1\,\omega^2/c^2}}{\varepsilon_2} + \frac{\sqrt{k_z^2 - \varepsilon_1\,\omega^2/c^2}}{\varepsilon_1} = 0 \tag{3.9}$$

On solving this equation the condition obtained for existence of SPP is $\varepsilon_1\varepsilon_2 < 0$. The above equation is solved with respect to k_z and following result is obtained

$$k_z = \frac{\omega}{c}\sqrt{\frac{\varepsilon_1\varepsilon_2}{\varepsilon_1 + \varepsilon_2}} \tag{3.10}$$

The eq. 3.10 is called the dispersion equation of Surface Plasmon Polariton.

3.6. Analysis of Dispersion equation of SPP

Let us take the two media combination of dielectric and metal as earlier and try to analyse the behaviour of electromagnetic field of this solution depending on propagation constant and frequency without solving Maxwell's equation. We know that for surface electromagnetic wave the field exponentially decayed in both the media

$$E, H \sim e^{-i\omega t + ik_z z}.\, e^{-\kappa_{1,2}\,|\,x\,|} \tag{3.11}$$

κ_1 and κ_2 are real and positive and so are their squared values. If κ^2 is negative it signifies that the exponentially decaying wave is transformed into propagating wave. Frequency controlled metallic dielectric constant is given as

$$\varepsilon_2 = \varepsilon_{2\infty} - \frac{\Omega_p^2}{\omega^2} \tag{3.12}$$

The expression for κ_2 after substituting the value of ε_2 is simplified into the following form

$$\kappa_2^2 = k_z^2 - \varepsilon_{2\infty}\frac{\omega^2}{c^2} + \frac{\Omega_p^2}{c^2} \tag{3.13}$$

On the basis of the values of κ_1^2 and κ_2^2 the whole dispersion plane is divided into three regions according to the behaviour of electromagnetic wave whether it is propagating or exponentially decaying.

In the Fig. 3.5 [39] the dashed lines are obtained by putting the expressions of κ_1 and κ_2 equal to zero. In the region-1 waves could propagate inside metal because it behaves as a dielectric and it is obvious since the frequencies in this region are higher than the plasma frequencies. All the waves are propagating waves in this region. Region-2, between the dashed lines, depicts the propagation of waves in dielectric medium and exponential behaviour inside metal. In the lower region which is the region-3, all the waves exhibit exponential nature. It means the dispersion of any surface wave should lie in this region.

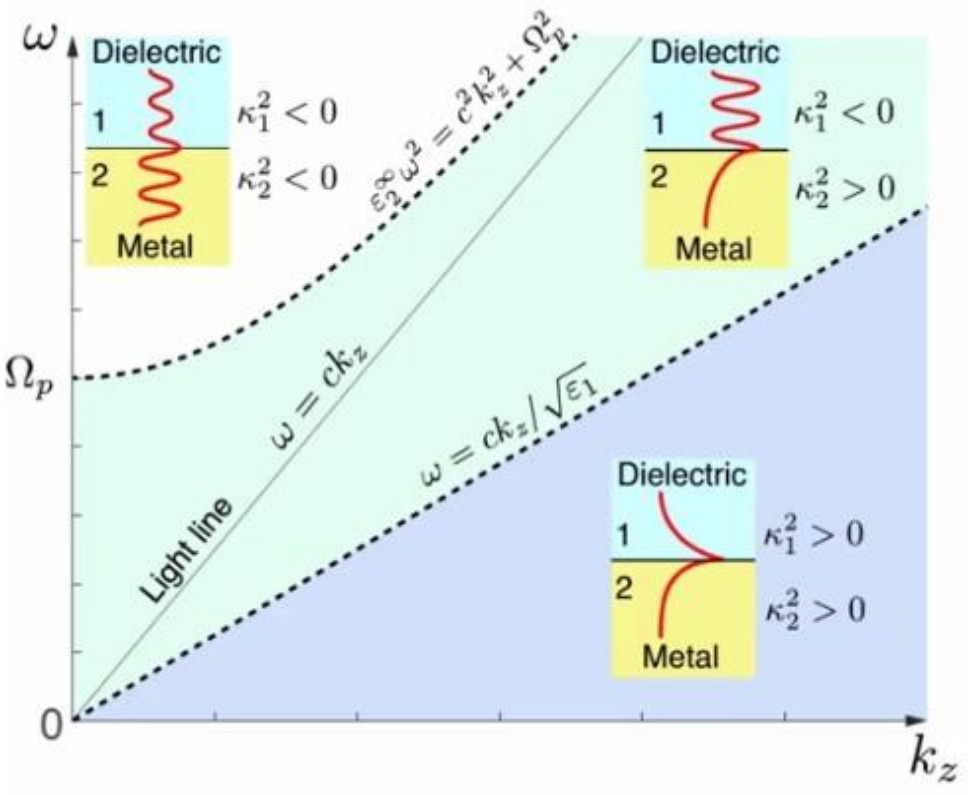

Figure 3.5: Analysis of Dispersion plane as reported in [39]

3.7.Solution of Dispersion Equation

By substituting the expressions of dielectric constants in the dispersion eq. 3.10 two solutions are obtained. The red branches in the Fig. 3.6 correspond to the solutions of

dispersion equation. Considering the upper branch, as it is clear this branch does not correspond to the surface wave because of its presence in the region where there is no localized surface wave and only propagating wave exists. This branch has a physical significance because it corresponds to a case when there is one propagating wave in each medium. It means there is an incident wave, a refracted wave but there is no reflected wave. This is the well-known Brewster Effect and this branch represents Brewster angle. Considering the lower branch, it can be seen that this branch corresponds to an exponentially decaying surface wave away from the interface inside both the media. This represents the dispersion of SPP. Fig. 3.6 [39] depicts important information on the nature of propagation of SPP at different frequencies. SPPs cannot propagate at low frequencies because there is no frequency cut off rate. Therefore, Surface Plasmon Polariton can be studied not only in visible or infra-red region, but also at far infra-red or even at terahertz frequencies. At lower frequencies the asymptote of SPP is linear shown by $\kappa_1 = 0$ line. At higher frequencies propagation constant grows at a very high rate and tends to infinity at some frequency. This frequency is called resonant frequency of Surface Plasmon Polariton denoted by Ω_{SPP}. This frequency can be calculated by equating the denominator of dispersion eq. 3.10 to zero i.e.

$$\varepsilon_1 + \varepsilon_2 = 0 \tag{3.14}$$

On solving, the resonant frequency of SPP is given by

$$\Omega_{SPP} = \frac{\Omega_P}{\sqrt{\varepsilon_1 + \varepsilon_{2\infty}}} \tag{3.15}$$

In the simplest case when both ε_1 and $\varepsilon_{2\infty}$ are equal to 1, then the resonant frequency is equal to plasma frequency of metal over square root of 2.

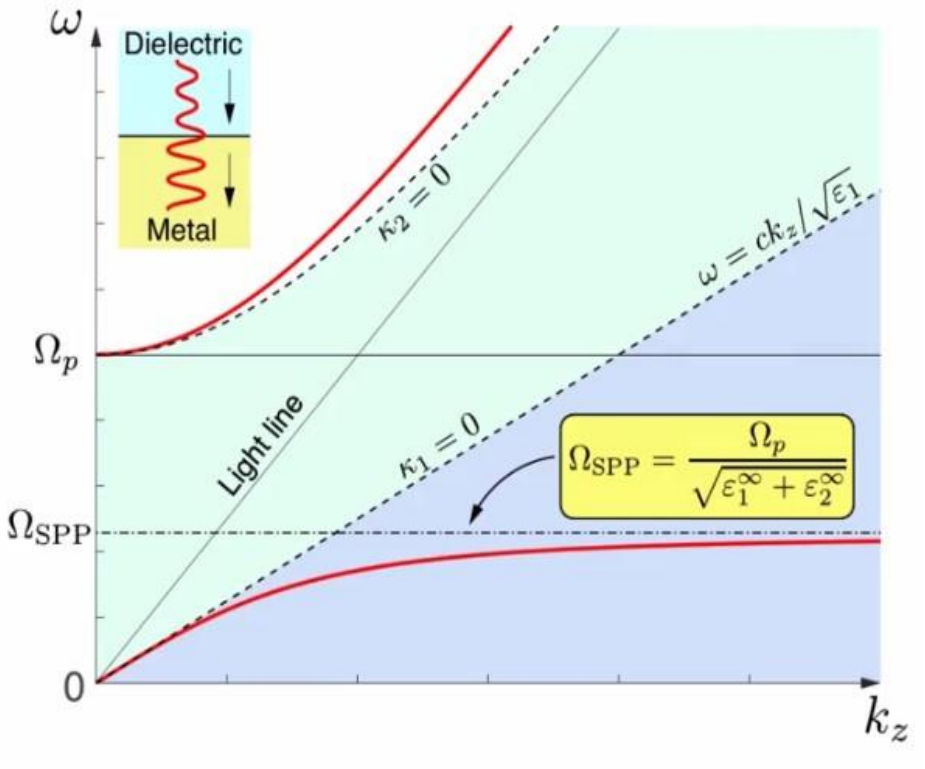

Figure 3.6: Solution of Dispersion Equation of SPP as reported in [39]

3.8.Excitation of SPP

As shown in Fig. 3.6, dispersion curve follows linear relationship in the low frequency regime and finally approaches the horizontal line in the high frequency region. For a given energy or frequency, it is found that the wave number k_z is invariably greater than the free space wave number. The enlarged value of wave number (or momentum) lies in the fact that there is a strong interaction between light and surface plasmons as a result of which the conduction electrons at the surface are carried by the light wave [46]. Therefore, SPP cannot be excited on metal-insulator interface through a free space photon due to the problem of momentum mismatch. To couple the photon into SPP its momentum has to be enhanced. Various phase matching techniques have been devised to alleviate this problem.

3.8.1. Prism Coupling

Prism Coupling is the most popular method for excitation of SPP. A thin film of metal is embedded between two dielectric mediums so that the wave vector gets increased by specific amount to match the momentum required for SPP generation. For simplicity, one of the mediums is taken as air. The in-plane momentum of the light reflected at metal-dielectric (prism) interface at an angle θ is given by $k_z = k_o\sqrt{\varepsilon_{prism}}\,\sin\theta$,

where ε_{prism} denotes the dielectric constant of the prism [46]. This momentum value is sufficient enough for SPPs to get excited at metal/air interface. This method of excitation is called attenuated total internal reflection. This method involves the process of tunnelling of fields of the impinging photons where SPP excitation occurs. Prism coupling is implemented using two configurations: Kretschmann Configuration and Otto Configuration.

In Otto configuration, metal film and prism are separated by a very thin layer of air. At the interface between prism and air total internal reflection occurs and the evanescent field enters the air-metal interface and excites SPP. The extent of coupling of evanescent wave totally depends on the thin air gap, so the separation should be carefully maintained. At a particular incident angle of the reflected light within the prism the momentum matching condition is achieved [14]. This configuration has the drawback of careful maintenance of air gap but is beneficial where straight contact with metal is avoided, as in the study field of surface quality.

Kretschmann configuration overcomes the limitation of the former method. In this approach, a direct contact between the prism and metal is maintained. Total Internal Reflection (TIR) occurs when the incident angle of the impinging photon beam is larger than the critical angle and the produced evanescent field moves through the nano-metallic film and reaches the metal-air interface where SPPs get excited (as shown in Fig. 3.7). The key factor is the metal thickness which determines the strength of evanescent signal reaching at metal end after penetrating through it. Higher the thickness of metallic film lower is the efficiency of SPP excitation owing to substantial sum of absorption losses in metal [14].

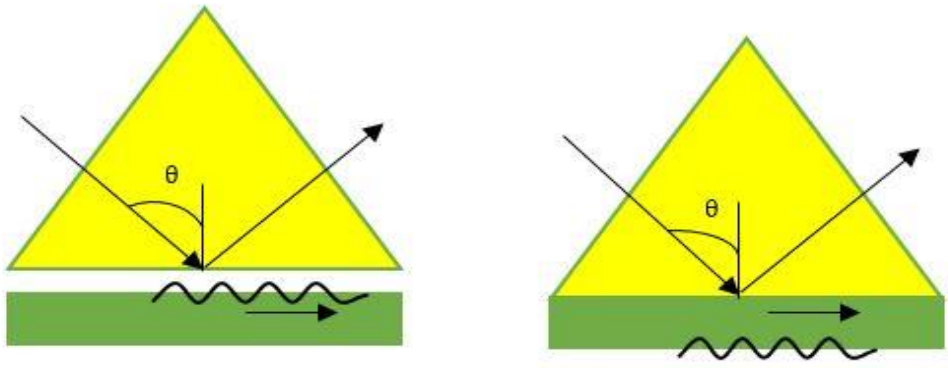

Figure 3.7: SPP excitation through prism coupling using a) Otto Configuration b) Kretschmann Configuration

3.8.2. Grating Coupling

Another way of achieving phase matching is through the use of grating surface [14]. By periodically distorting the metal-dielectric interface, the incident light is diffracted resulting in series of light beams direct at different angles. If the total momentum component of these beams matches with that of wave-vector (momentum) k_z, SPPs are generated. Fig. 3.8 depicts simple 1D grating of grooves, the phase matching occurs when

$$k_z = k\,sin\theta \pm mg \tag{3.16}$$

Where $g = \frac{2\pi}{a}$ denotes the grating reciprocal vector, a is the lattice constant and m is a positive integer . When the intensity of the reflected light is minimum it is the indication of the excitation of SPP.

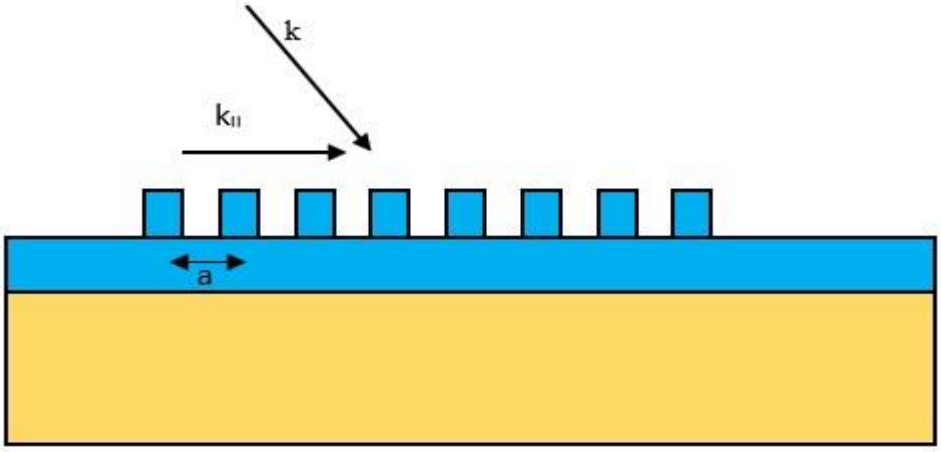

Figure 3.8: SPP excitation in grating through phase matching as reported in [14]

3.8.3. Excitation using highly focused optical beams

A variant of the conventional prism method, a microscope objective having large numerical aperture (NA) can also be used for SPP excitation at the metal/dielectric interface. Fig. 3.9 displays the setup for excitation. A direct contact is made between an oil-immersion objective and a glass (dielectric) substrate. The role of the immersion layer is to match the index for fulfilling the resonance condition. As the NA is quite high the focused excitation beam shows a large angular spread including angles larger than the critical angle. After the excitation, at an angle larger than the critical angle, in the form of leakage beam the SPPs radiate back into the glass. This focused beam and the angular regulation is responsible to excite SPPs at diverse frequencies [14].

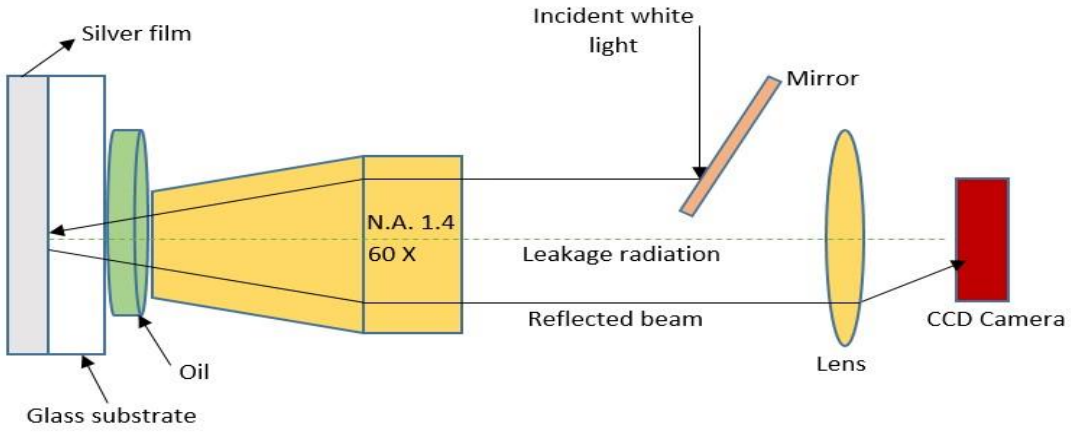

Figure 3.9: SPP excitation using highly focussed optical beams as reported in [14]

3.9.Multiple Metal/Dielectric Interface

In the above methods the excitation is alongside the single metal/dielectric interface. As metal suffers from large ohmic losses, after propagating very small distance (on the order of few μm) the SPPs eventually vanish. It is possible to excite SPP modes in multiple metal/dielectric interface geometries since these arrangements play a key role in long distance communication. The constructive and destructive interference between modes generate SPP along the interface of sandwiched layer. At both the interfaces SPPs are generated and if the insulating layer is quite narrow then the SPPs get coupled yield coupled gap SPPs (GSPPs). GSPPs exhibit attractive properties that are helpful in applications involving optical ICs. The propagation of SPPs is shown in Fig. 3.10. Multiple metal/dielectric structures can be categorized into two types: Insulator-metal-insulator (IMI) and Metal-insulator-metal (MIM) waveguides.

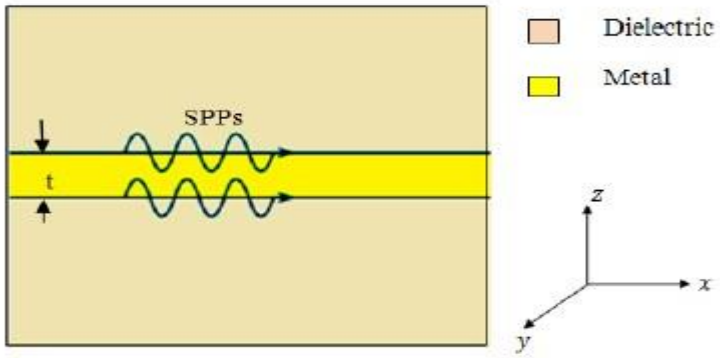

Figure 3.10: SPP excitation in multilayer structure with metal layer embedded between dielectric mediums as reported in [46]

3.9.1. Insulator-Metal-Insulator (IMI) structure

This waveguide geometry contains a tiny layer of metal embedded between two insulating layers having same or different dielectric constants. This waveguide structure is very useful when distance separating the interfaces is of the order of decay length of the evanescent field inside metal. The thickness of the metallic layer is properly selected so that the exponentially decreasing field that supports the SPP at one interface can couple with a surface plasmon mode at the other surface interface [11]. At both the interfaces the propagation frequency of the SPPs is same and the evanescent tails of the SPP modes overlap and result in constructive and destructive coupling. Two bound SPP modes are generated – a symmetric low frequency even mode and an asymmetric high frequency mode [47]. The propagating wave-vectors for both the modes are different. In the symmetric mode the in plane magnetic field component perpendicular to direction of propagation and the transverse electric field component show a symmetrical distribution while asymmetric modes exhibit asymmetrical distribution. The IMI waveguide is characterized by minor loss and longer length of SPP propagation but suffers from the disadvantage of poor light confinement into sub-wavelength structures.

3.9.2. Metal-Insulator-Metal (MIM) structure

In this configuration, in between two metallic layers a thin layer of insulating material is sandwiched. The electromagnetic mode propagates in the form of coupled SPPs and this mode is confined in sub-wavelength scale [48]. The coupling of the SPP modes is totally dependent on the thickness of the insulating layer. When the thickness is large enough the SPP modes propagate independently along both the metal/insulator interfaces without any interaction but as the insulating layer becomes small in size the two SPP modes couple with each other to generate gap SPP modes. MIM waveguide simultaneously supports three guided modes- forward propagating symmetric, antisymmetric SPP mode and backward propagating anti-symmetric SPP mode. The backward propagating SPP mode shows huge propagation losses and is used at optical frequencies for realizing negative refraction [49]. Thus, symmetric modes exist in MIM waveguides having symmetrical and asymmetrical distributions of transverse components and longitudinal components of the electric field respectively. MIM waveguide having the mentioned field distribution is known as Plasmonics slot waveguides. For the plasmonics mode, the dispersion relation is given by [50]:

$$\tanh(k_{z,d}\frac{t}{2}) = \frac{\varepsilon_d k_{z,m}}{\varepsilon_m k_{z,d}} \quad (3.17)$$

Where $k_{z,m(d)} = \sqrt{k_{G-SPP}^2 - \varepsilon_{m(d)} k_o^2}$, here k_{G-SPP} is the propagation constant for propagating wave in Plasmonics slot waveguide. As the insulating layer gets narrow the propagation constant of GSPP mode increases largely and there is lateral confinement of the mode in sub-wavelength scale with the disadvantage of reduced propagation length. It clearly indicates the inverse proportionality between the propagation loss and SPP mode confinement. When the system is switched from uncoupled mode to coupled mode and the thickness of dielectric material is decreased, the propagation length initially increases. For MIM waveguide based GSPPs, the propagation length is approximately 8% higher than that of independent SPPs along single metal/insulator interface (an uncoupled system). The length of propagation of SPP in MIM structure is dependent on the insulator thickness. As the width of dielectric reduces the electric field of GSPP resembles the electrostatic nature [51].

Consequently, the concentrated electric field in the gap varies according to the thickness of the gap. Initially there is a rise in the electric field and it attains the highest value and then gradually it starts to drop as a result of its squeezing from the insulating gap into metal. In case of excitation for frequencies lower than the bulk plasmon frequency, GSPP mode lets the propagation of SPP with an enlarged propagation constant. These characteristics of GSPP are utilised in designing of GSPP based waveguide structures such as Bragg gratings, wedges etc. [25,52].

3.10. Applications of MIM based SPP waveguides

The appealing feature of confining signal at sub-wavelength scale in MIM waveguide offers ultra-small foot-print. Therefore, considering all the benefits of MIM waveguide, it is considered as the best choice for designing highly integrated photonic circuits. Because of the merit of overwhelming the diffraction limit, MIM waveguide is extensively used in various applications based on photonic devices like as:

i. Refractive Index sensors
ii. Bragg Reflectors
iii. Optical filters
iv. Optical Multiplexer/ Demultiplexer
v. Optical Switching
vi. Slow light generation

3.11. Fano resonance and its applications in Plasmonics System

A resonance in the system is indicated as a magnification in the magnitude response when the input excitation frequency matches with the system eigen frequency. This matching results in a sudden surge in the amplitude response of the system towards its maximum value. There is a phase shift of π radians at resonance condition [53]. The resonance profile is symmetrical and is explained using Lorentzian profile functions and is totally contrasting from Fano resonance used for the characterization of resonance exhibiting asymmetrical profile. The underlying physics behind Fano resonance can be comprehended by the modelling of two harmonic oscillators coupled together wherein a periodic force drives one of the oscillators while the other oscillator is driven by the first one [53-54]. The proximity in the eigen frequency of both the oscillators results in interference which gives rise to asymmetrical shaped resonance. In the recent years, researchers have come up with novel avenues for the excitation of Fano resonance in the Terahertz regime by employing plasmonics [55], photonic crystals [56] and metamaterials [57]. The ability of Fano resonance to confine light in sub wavelength scale and overcome the diffraction limit has triggered a huge interest in SPP based Nanophotonics. Many plasmonics based waveguide structures have been reported previously to achieve Fano resonance [57-59].

3.11.1. History

In 1902 asymmetrically shaped lines were traced by Wood [60]. When white light is incident on a metallic grating, the optical spectrum shows some bright or dark bands. For a certain wavelength range the spectrum is highly intense and all of a sudden the intensity falls to near zero for a short range of wavelength. The dark mode has a narrow spectral width of the order of the separation between two sodium D-lines. Wood's experiments resulted in a single D-line under certain lighting conditions.

The quick fall in the level of intensity for narrow spectral regime was referred as Wood's anomalies as the conventional theory of grating failed to justify this effect [61]. Later in 1907, Lord Rayleigh in his work "On the dynamical theory of gratings" addressed this anomaly. He built his work on the EM field expansion in radiative fields [62]. The drawback of his theory was it only provided that wavelength value at which D-line was noticed and that wavelength was dubbed as Rayleigh wavelength. But his work could not explain the logic behind the asymmetrical resonance spectrum.

An Italian physicist Ugo Fano in his series of experiments addressed this problem and could solve it [63-65]. By extending the theory of grating by Rayleigh, Fano suggested that the best way to define anomaly is by using the concept of surface wave excitation along the grating. The phase matching between the incident and guided waves lead to the excitation of evanescent wave resonantly near the grating which in turn enhances the field near the grating surface. Along the grating surface the guides modes interfere with the propagating evanescent or leaky surface waves in such a way that over a small frequency range the minimum and maximum intensity values are observed along with a resonance profile that is asymmetrical.

Fano resonance was observed for the first time in the extraordinary transmission through metallic films and since then this phenomenon is widely used in several nano-plasmonics and nano-photonics systems. As explained in Chapter 3, MIM waveguide based systems are capable of guiding light beyond the diffraction limit and hence optimum for on-chip optical device designing. If the phenomenon of Fano interference is excited in Plasmonics based waveguides, the performance of some optical devices can be greatly improved.

This is the reason behind the extensive study of Fano resonance in Plasmonics systems. The asymmetrical profile characterized with sharp dispersion makes the Fano resonance highly convenient for various applications viz. optical switching [66], electromagnetically induced transparency (EIT) [67], biosensing [68] and many more. The next section deals with the comprehensive discussion of Fano resonance in Plasmonics systems.

3.11.2. Fano resonance in Plasmonic System

Fano interference modelling in Plasmonics systems is explained either classically or quantum mechanically. In the view of Quantum mechanics, this resonance results from the interference between quasi-discrete energy state and continuum spectrum of elementary excitations. Since this phenomenon occurs at micro and nano levels, so it stands as a huge challenge from the classical point of view. But, nowadays Fano interference has gained popularity and is implemented classically in metamaterials [57], coupled cavities [11] and also in plasmonics based systems [55]. In plasmonics, the interaction between a localized or dark mode and a radiative or bright mode results in Fano resonance. The far-field of the plane wave illumination excites the bright mode. Whereas the dark mode is not directly excited through the illumination field rather the near-field of the bright mode is responsible for its excitation. Hence, the bright mode is

directly excited by illumination field which in turns excite the dark mode. There is interference between the dark and bright modes. The nature of the response of the bright mode totally depends on the phase difference between these two pathways. Accordingly, the response could either strengthen or weaken. Since the excitation frequency controls this relative phase, the system shows an asymmetric line shape.

This resonance based on Fano interference differs from the Lorentzian shaped resonance on the grounds of the profile shape as systems exhibiting Fano resonance exhibit asymmetric profile [53-54]. This asymmetrical resonance profile results in a large Q-factor. By modifying the structural and optical parameters, the alteration of the Fano resonance profile becomes easy. The sharp transition provided by Fano resonance in frequency spectrum is widely studied in the domain of frequency sensitive applications [69-70].

This effect can be excited in Plasmonics system by two ways: Firstly, when the symmetry of the perfect structure is broken as in Plasmonics metasurfaces [57], asymmetric stubs in MIM structures [29,55] and asymmetric shaped single slit [71]. Secondly, by the use of the coupled-resonator system such as cavity-cavity interference [72], coupling of Plasmonics nanoclusters [73] etc. In coupled Plasmonics system the excitation of Fano resonance is due to the hybridization of various plasmon modes. These hybridized modes are classified into bright and dark modes []. Due to the ability of the bright modes to couple with EM excitations, they radiate efficiently and hence are spectrally broad. On the other hand, the dark modes are not spectrally broad and are weakly coupled to incident excitation. As a result of this coupling the resonance spectrum exhibits a transparent window, where the reflectivity sharply falls to a minimum value. The coupling and interference between both the modes is necessary for excitation of Fano resonance [53,55,57].

3.12. Conclusion

With the ever increasing demand of high speed information processing the performance of traditional electronic ICs is not up to par. The photonic circuits have opened up the avenues to manipulate the propagation of optical signal in the chip scale of the order of micrometer but there is a clear mismatch in size between the micrometer scaled photonic circuits and their nanometer scaled electronic counterparts. The diffraction limit governs the minimum size of the photonic circuits. Hence SPPs propagating at the metal/dielectric interface offer fascinating ways to confine and guide the optical signal

via highly localized surface waves. Light confinement in deep subwavelength scale is supported by MIM and IMI waveguide structures. MIM waveguides are better candidates for confining light in sub-wavelength range and are widely used in the fields of sensing, buffering, switching etc.

4. ANALYSIS OF MIM BASED PLASMONIC GRATING AND ITS APPLICATIONS

In this thesis, we have designed different MIM based grating structures for obtaining band stop filtering characteristics. We will analyse the band stop characteristics of different geometries one by one and then design a perfect Plasmonic grating whose applications in band stop filtering, multiple switching and refractive index sensing are discussed thoroughly.

4.1. MIM grating with stubs having lateral orientation

In this configuration the stub resonators are placed directly on the insulating layer as shown in Fig. 4.1. The stub resonators are arranged in a periodic fashion with a unit cell section of length 670 nm. The stub length equals 450 nm with 220 nm separation while

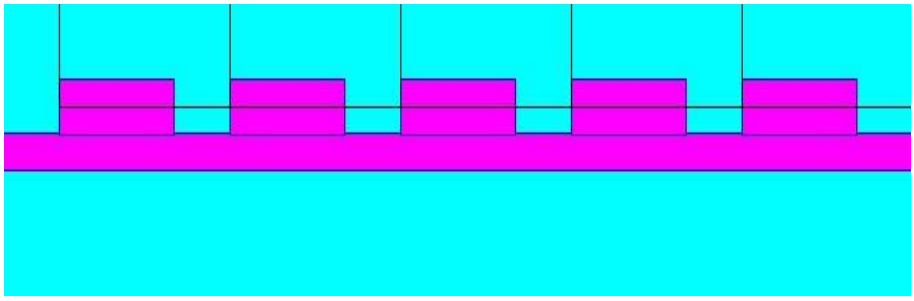

Figure 4.1: MIM grating with laterally oriented stubs

the width of the insulating layer is kept at 100 nm. The incident light is Gaussian modulated and the wavelength used is 1550 nm and the material of resonator and the insulating layer is air. The metal used is silver because it exhibits the least absorption. The permittivity of silver is modelled using Drude formula stated in eq. 3.4. Table 4.1 lists the Drude parameters defined for silver.

Table 4.1: Drude parameters of Silver

Parameters	Values
ε_∞	3.7
γ	2.73×10^{17} Hz
Ω_p	1.38×10^{16} Hz
λ	1550 nm

The simulations are performed using the method of Finite Difference Time Domain (FDTD). The transmission spectra for different periodicity of cells is plotted in Fig. 4.2. The waveguide shows good filtering characteristics. It is clear that with the increase in period number N the transmission around the central wavelength goes down.

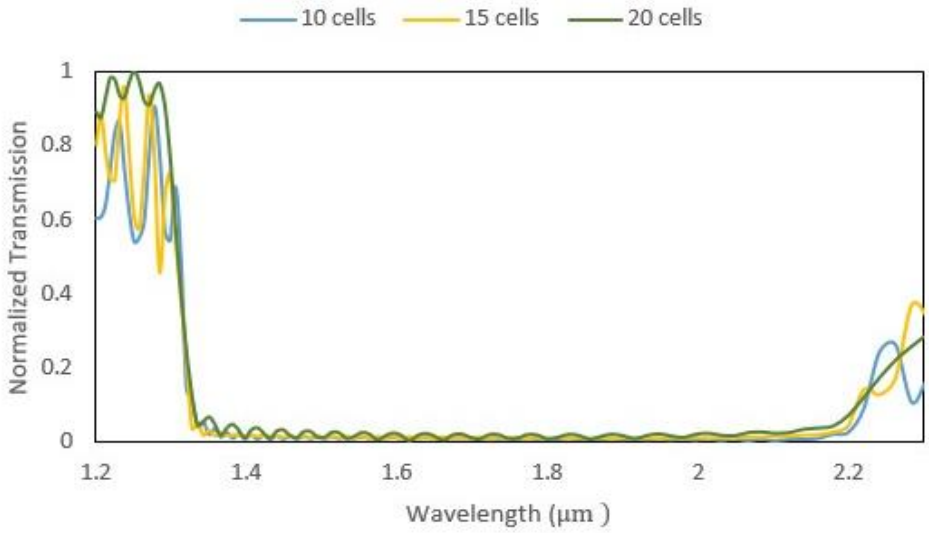

Figure 4.2: Transmission Spectra of MIM grating for different period number

4.2. MIM grating with stubs having transverse orientation

In this configuration, the stub resonators are oriented in a perpendicular direction. This arrangement has the interchanged values of the stub dimensions as compared with the previous design as shown in Fig. 4.3.

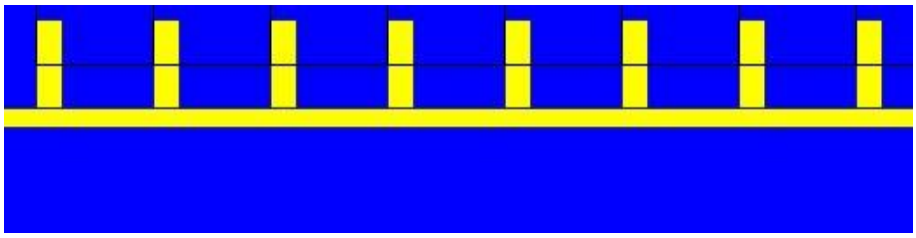

Figure 4.3: MIM grating having transverse orientation of stubs

Fig. 4.4 and Fig. 4.5 depict the transmission spectra and the magnetic field distribution respectively. It can be concluded by observing the transmission spectra that as the period number goes up the transmission goes down. Although the stop band obtained is narrow as compared with the last design but with the increase in the period number the ripples in the stop band are tuned and more flat stop band is achieved moving from N=10 to N=15.

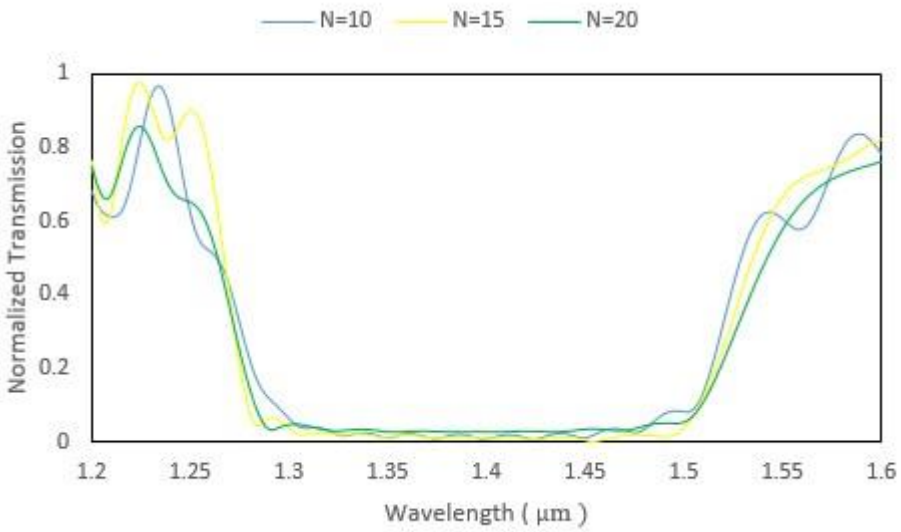

Figure 4. 4: Transmission Spectra of MIM grating with different period number

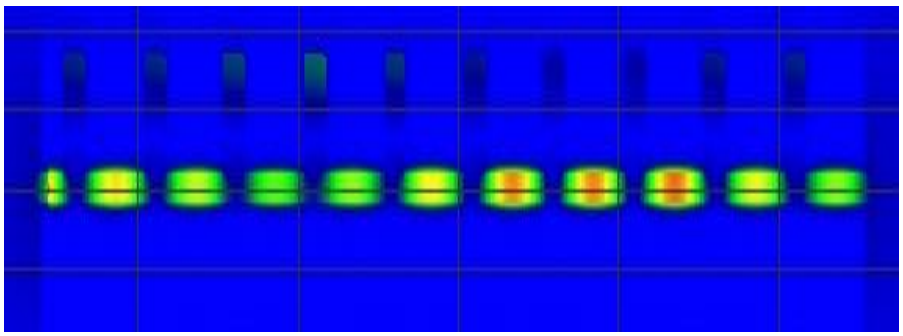

Figure 4.5: Magnetic field distribution

4.3. MIM grating with stubs positioned at the centre of the insulator

This configuration has the stubs arranged in a parallel manner with equal widths lying above and underneath the insulating portion. It should be kept in mind that the metal possesses negative refractive index and with the increase in the insulator width the effective refractive index of the MIM waveguide gradually decreases. As we will see in the upcoming configurations that since the insulator occupies more space in the waveguide in this design, the width of the stop band is more in this design than in the

other waveguide configurations. Fig. 4.6 and Fig. 4.7 show the arrangement and the transmission characteristics for N=9 respectively.

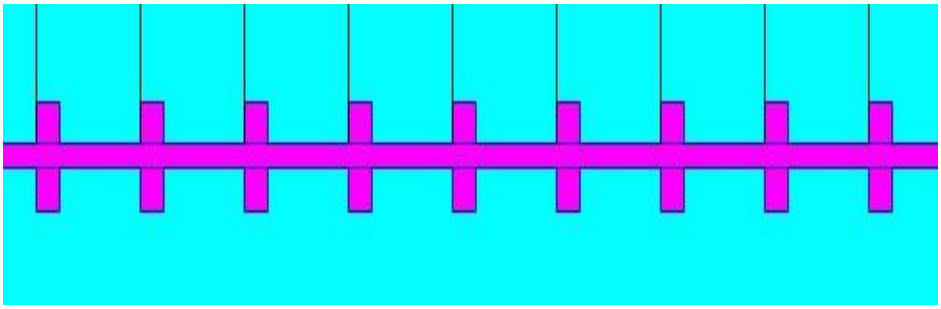

Figure 4.6: MIM grating with parallel orientation of stubs

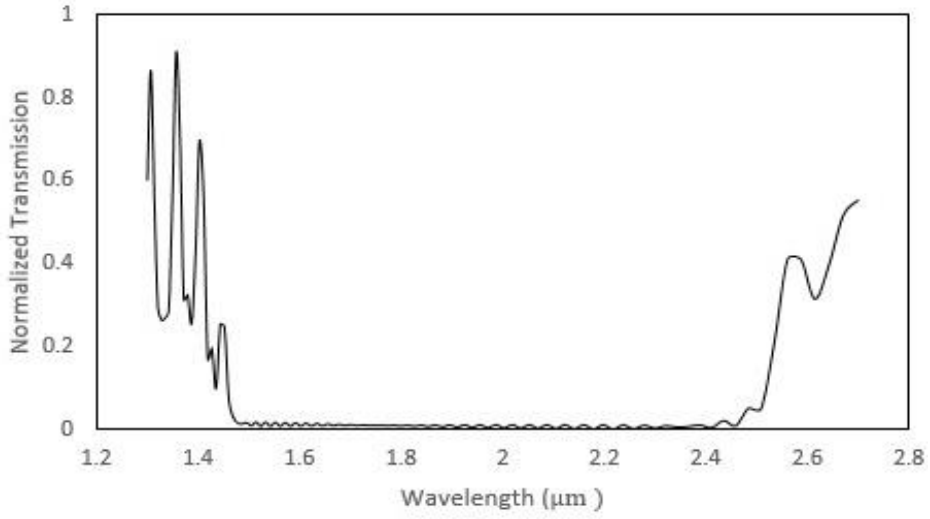

Figure 4.7: Transmission spectra for N=9

4.4. MIM grating with tapered arrangement of stubs

This arrangement comprises of two designs, one in which the stub resonators are arranged in increasing order of the widths and the other in their decreasing order of widths. The adjacent resonators vary in width by 20 nm as plotted in Fig. 4.8 and Fig. 4.10.

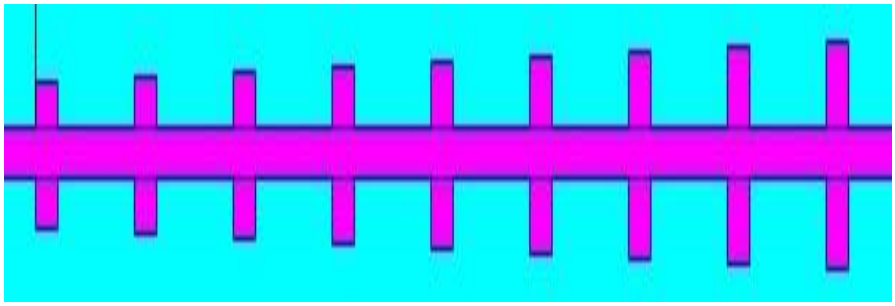

Figure 4. 8: MIM grating with Stubs arranged in increasing order of widths

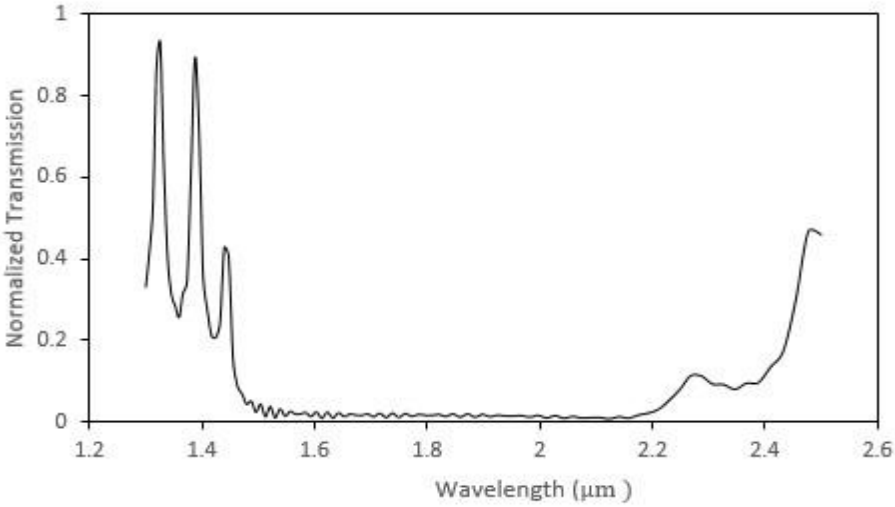

Figure 4.9: Transmission spectrum of increasing grating for N=9

As can be seen that the resonator width gradually increases along the length of the insulator. The spread of the stop band is reduced owing to the fact that the overall effective refractive index decreases with increasing width as shown in Fig. 4.9 and Fig. 4.11.

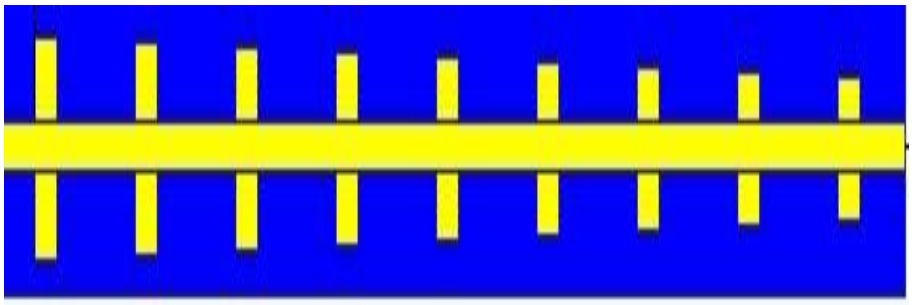

Figure 4.10: MIM grating with Stubs arranged in decreasing order of widths

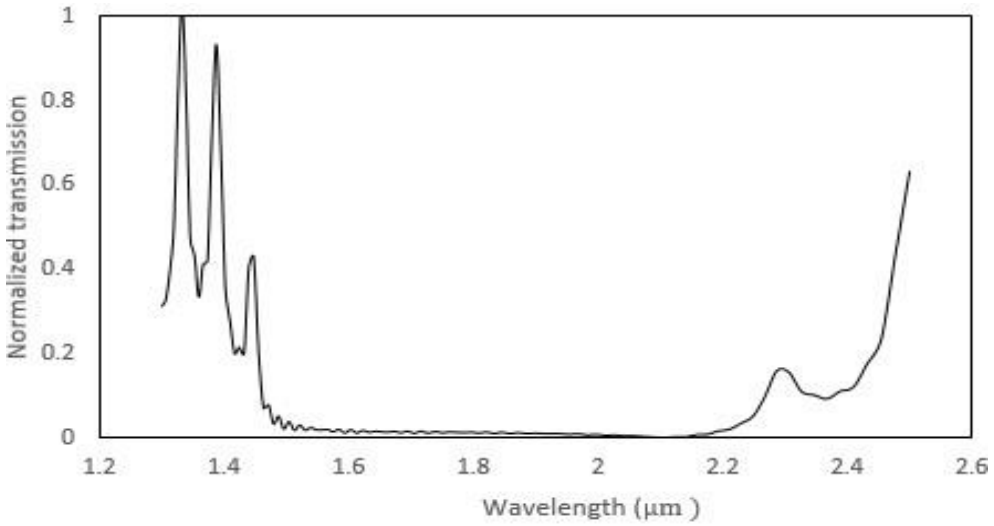

Figure 4.11: MIM grating with Stubs arranged in decreasing order of widths

4.5. MIM based perfect Plasmonic grating

A plasmonic grating is formed by periodically modulating the insulator width in a MIM waveguide structure. The plasmonic grating is analogous to a fibre Bragg grating and is designed to stop a band of frequencies. The structure comprises a MIM waveguide having a periodic arrangement of insulating regions P_1 and P_2 as plotted in Fig. 4.12. The metallic portion is made of silver as it offers lowest absorption loss as compared with other noble metals. The permittivity of silver is modelled using Drude formula stated in eq. 3.4.

As the plasmonic grating is behaving as a reflector, the Bragg condition around the central wavelength is given as follows [25]:

$$k_o[n_1 L_2 + n_2 L_1] = (2m + 1)\pi \qquad (4.1)$$

where $k_o = \frac{2\pi}{\lambda}$ is the propagation constant of central wavelength of the stop band (here λ=1550 nm) , L_1 denotes the length of resonator while L_2 is the separation between adjacent resonators, n_1 and n_2 represent the effective refractive indices of the resonator and the insulating portion that separates consecutive resonators, respectively. The values of the effective indices can be obtained from the relation given as [25]:

$$\tanh\left(\frac{1}{2}\alpha_1 d\right) = -\frac{\varepsilon_1 \alpha_2}{\varepsilon_2 \alpha_1} \qquad (4.2)$$

The dielectric constants of the insulator and metal are represented by ε_1 and ε_2 respectively. d represents the insulator width, α_1 and α_2 are the wave-vectors in the

transverse direction for insulating and metallic portion respectively, whose dependence with effective refractive index n is given by

$$\alpha_i = \sqrt{(n^2 k_o^2 - \varepsilon_i k_o^2)} \tag{4.3}$$

Using above two eq. 4.2 and 4.3, the relation between n and the width of the insulator layer has been reported in [25]. Thus, by increasing the width of the insulating portion of MIM waveguide, effective index decreases. Table 4.2 reports the values of the geometrical parameters.

Table 4.2: Structural parameters of Plasmonic grating

Parameters	Values (nm)
L_1	450
L_2	220
W_1	150
W_2	100

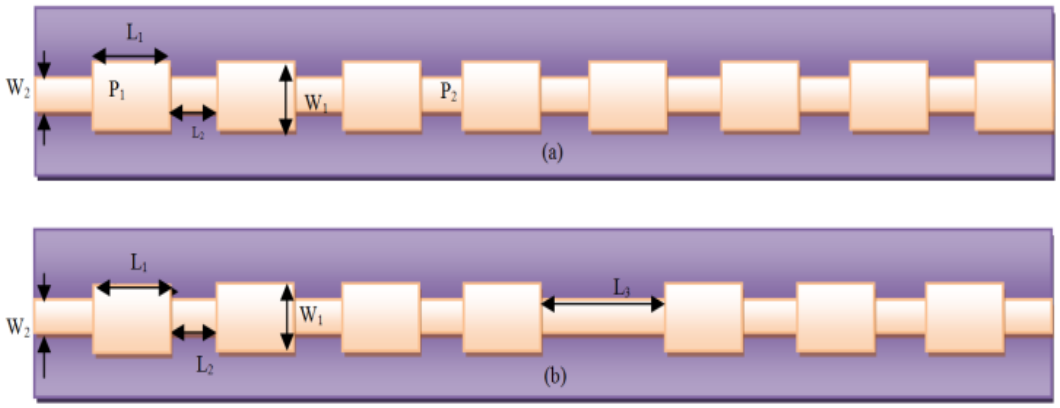

Figure 4.12: (a) Plasmonic grating with periodic resonators (dimension W1×L1) separated by distance L2 (b) Plasmonic grating with periodic resonators (dimension W1×L1) separated by distance L2 and having defect region with length L3

The proposed structure is simulated using FDTD with the following simulation parameters: The boundary condition is perfectly matched layer (PML). The size of the spatial steps is selected to be $\Delta x \times \Delta z = 5$ nm × 2 nm and the time step is specified as

mentioned in [29]. On launching Gaussian modulated continuous wave at the input, surface plasmon mode is excited at silver-air interface.

Fig 4.13 (a) plots the transmission spectrum of the perfect plasmonic grating (without defect). It is clear that the plasmonic grating operates as a filter with a stop-band centered near the central wavelength 1550nm characterized by a minute transmission. But as the defect region is introduced in the perfect plasmonic grating by increasing the length of the resonator, a special mode (known as defect mode) is allowed in the stop band of the grating as shown in Fig. 4.14. The frequency of the defect mode can be tuned by tailoring the defect region length. Therefore, the defect mode of the plasmonic grating is viable for filtering, demultiplexing or sensing based application.

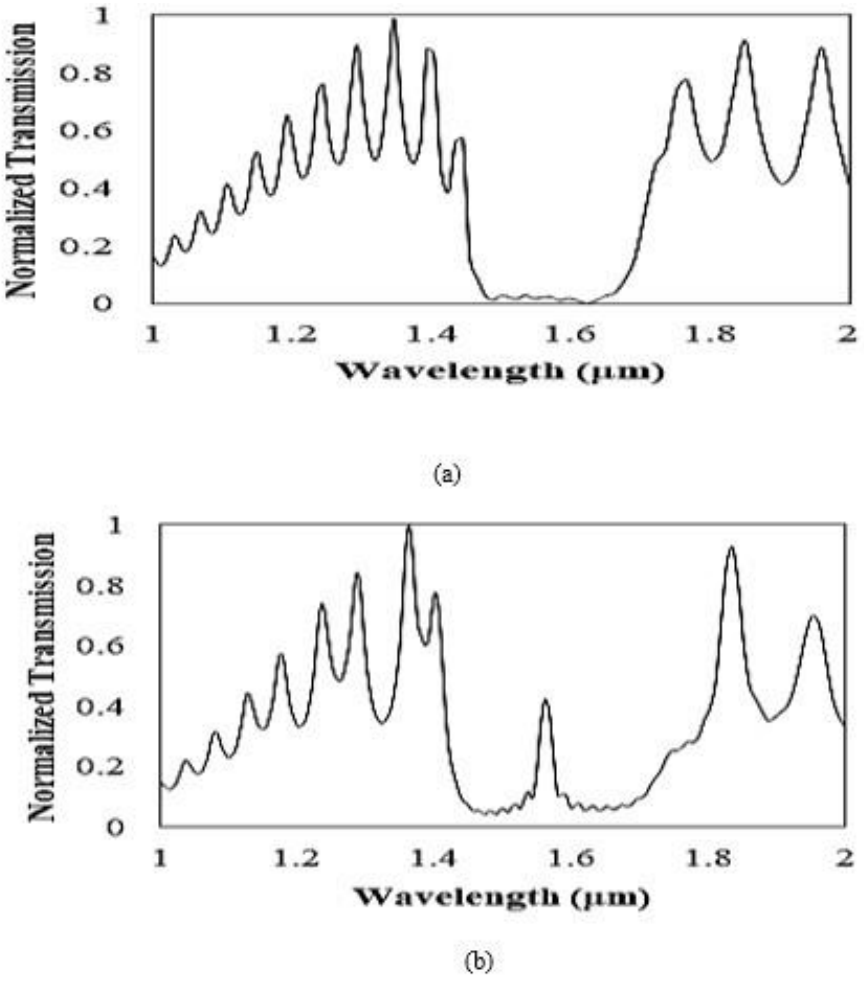

Figure 4.13:(a) Transmission spectrum of plasmonic grating having 18 cells section. (b) Transmission spectrum with a defect length equal to 550 nm having periodicity of 7 on both sides.

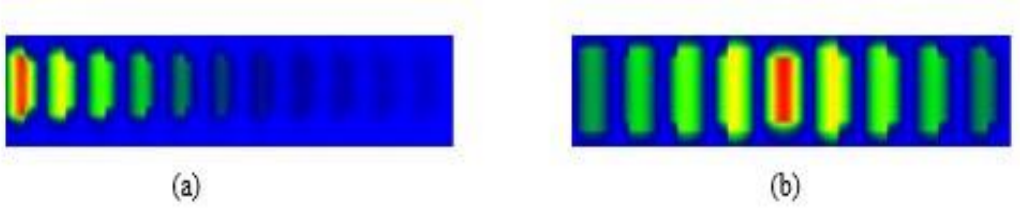

Figure 4.14: (a) Magnetic field profile of plasmonic grating without defect (b) Magnetic field profile of plasmonic grating with defect

The quality of the device is analysed using a performance measuring unit i.e. Quality factor which is stated as the ratio of the incident wavelength to 3 dB bandwidth of reflection. Quality factor (Q-factor) is given by:

$$Q = \frac{\lambda}{\Delta\lambda}$$

The Q- factor of the narrow window is found to be 85.12. The Q-factor is tunable by varying the structural parameters (height and width of the stubs).

4.5.1. Effect of structural parameters on transmission spectra

It is obvious, as the grating periodicity N rises, the transmission dip gets deeper approaching near zero which is similar to fibre Bragg grating (FBG). It can be seen that as the number of periods are increased the side lobes become more pronounced. These large side lobes arise via light scattering at abrupt change in refractive index between narrow and wide portions of the insulating regions.

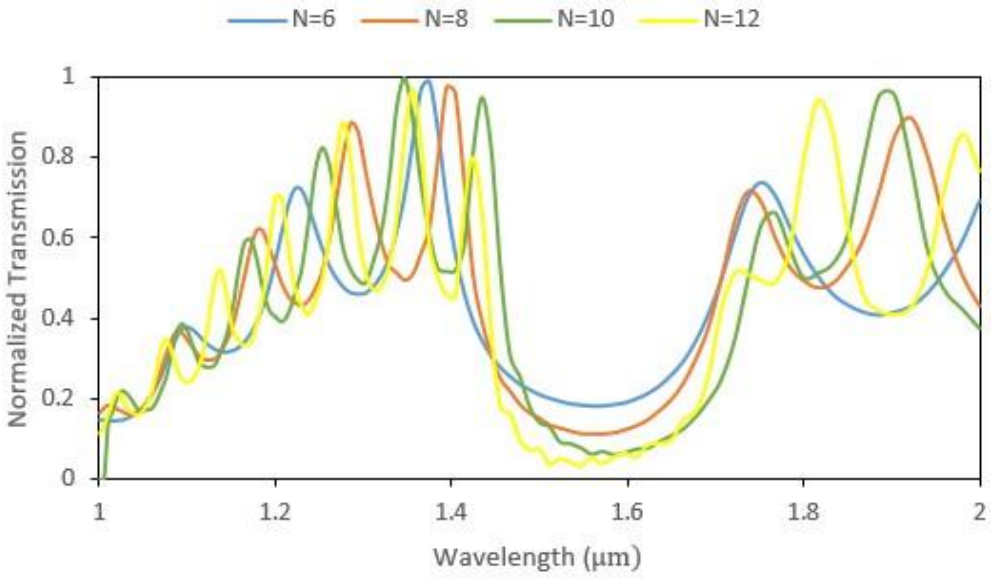

Figure 4.15: Transmission spectra for different period number

Fig. 4.16 shows the variation in transmission spectra for different insulating widths for N=8. As the width is reduced the central wavelength is red shifted from 1.51 μm to 1.61 μm with a widened stop band. This is due to the fact that there is indirect proportionality of the effective index and the insulator width as a result of which the width of the stop band gets reduced.

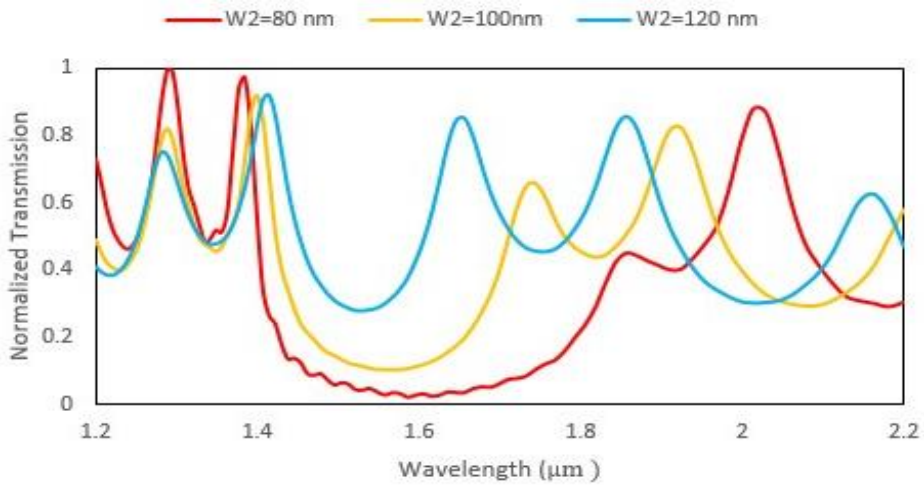

Figure 4.16: Transmission spectra for different widths of the insulating region

The transmission characteristics for various stub lengths is plotted in Fig. 4.17. As the length increases the stop band gets shifted to the right which is in accordance with the Bragg condition. Fig. 4.18 plots the central wavelength variation of the stop band with the stub length.

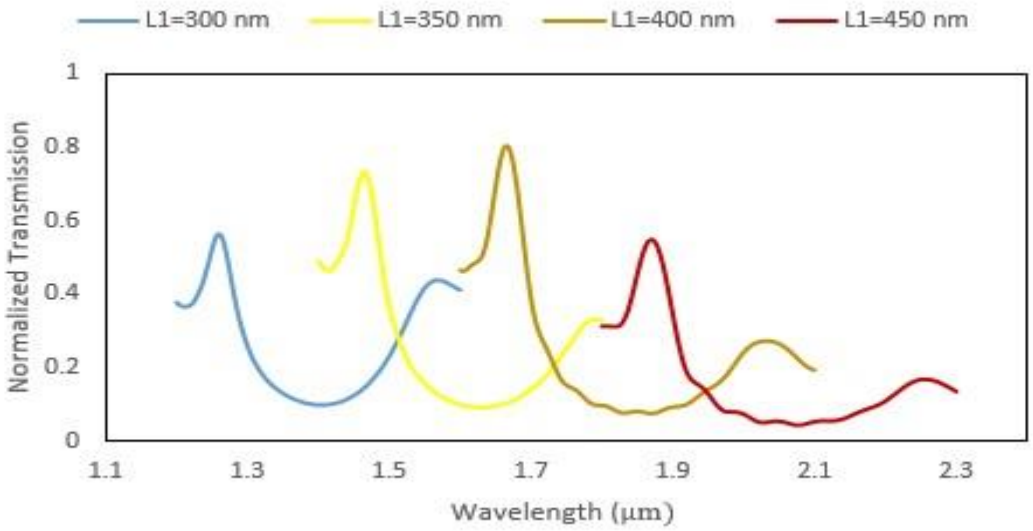

Figure 4.17: Transmission spectra for different lengths of the stub resonator

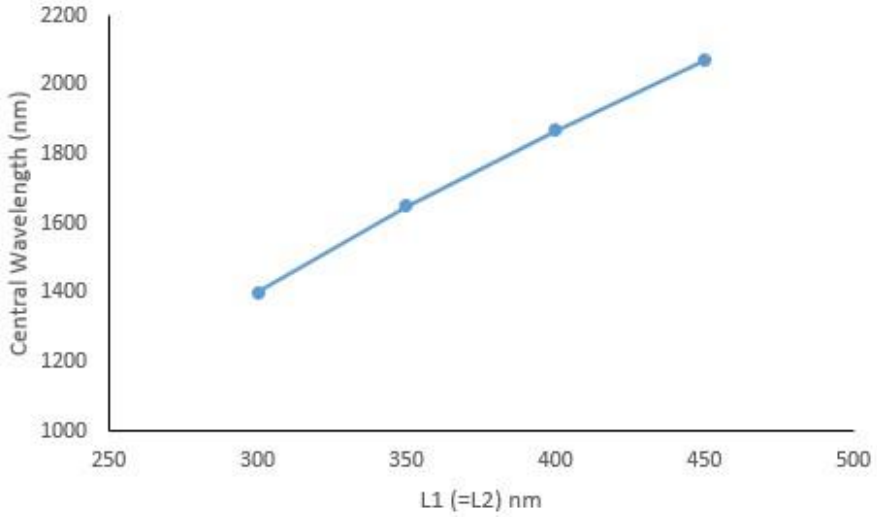

Figure 4.18: Central wavelength as a function of the stub length

It is noticeable from Fig. 4.19 that there is a red shift in the spectra with the defect mode peak tending towards longer wavelengths as the defect length increases. Fig. 4.20 plots the variation of the defect wavelength with the defect length.

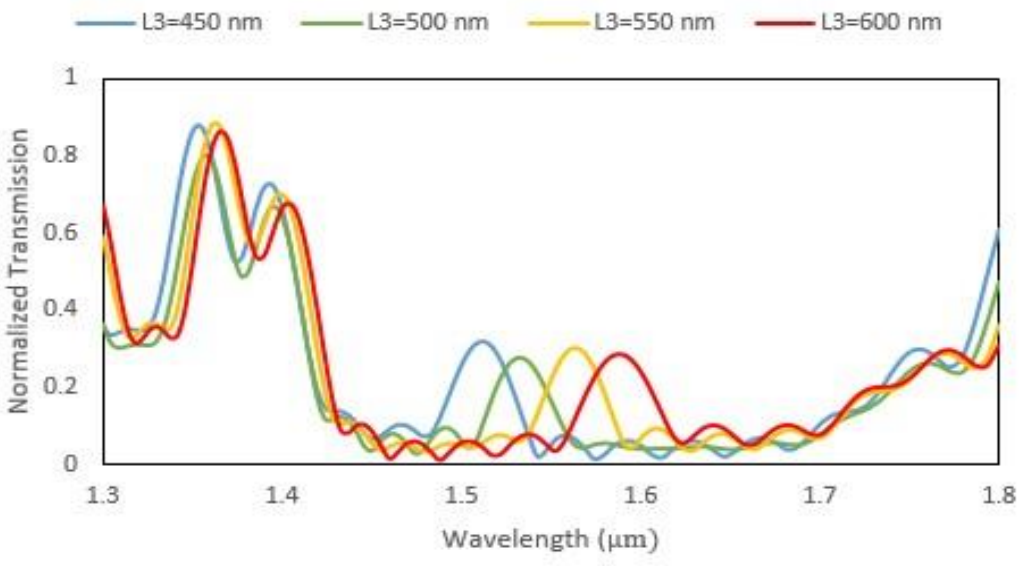

Figure 4.19: Transmission spectra with different defect lengths

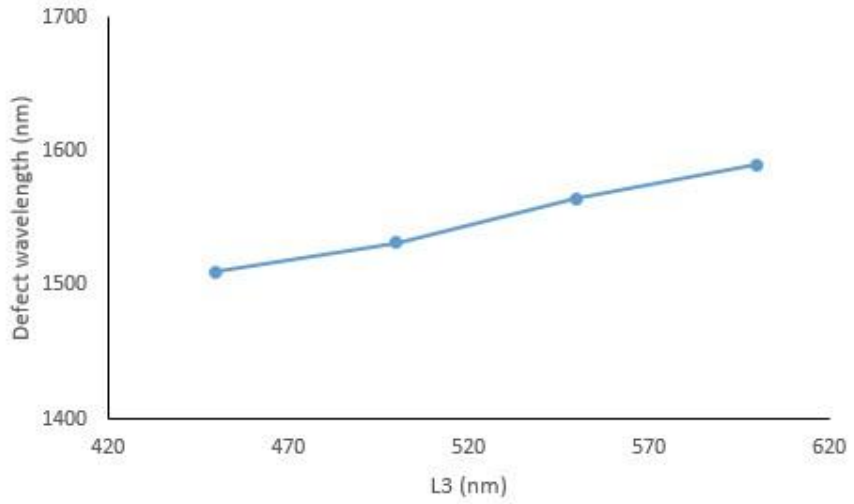

Figure 4.20: Central wavelength as a function of the defect length

We see how the intensity of the defect mode is effected by the width of the insulator connecting the stub resonators. As the insulator width increases more number of modes are excited in the waveguide. Due to which the intensity of the defect mode enhances as shown in Fig. 4.21.

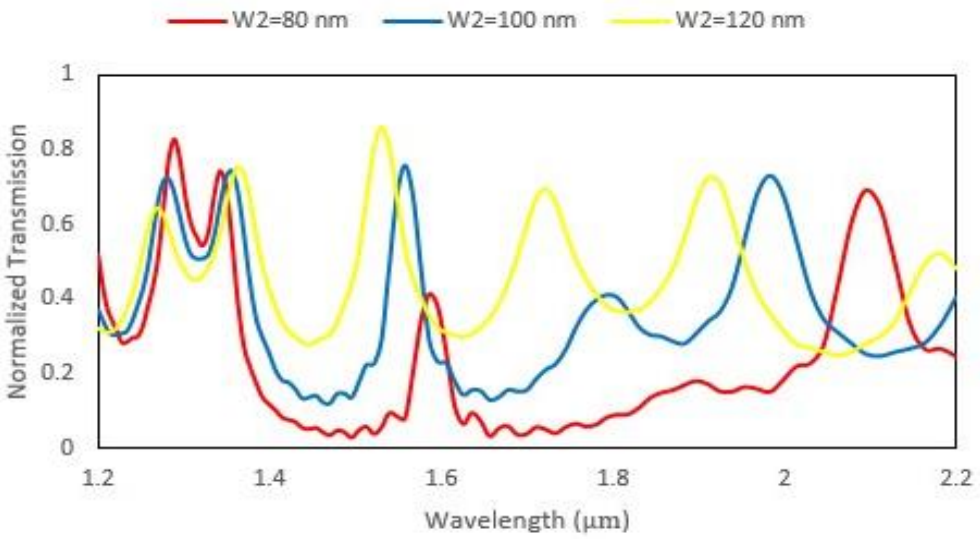

Figure 4.21: Transmission spectra as a function of width of the insulating region

4.6. Fano resonance excited Plasmonic grating filter

When the plasmonic grating is loaded with a silver nano-slit of 10 nm thickness in the defect region as depicted in Fig. 4.22, the resonance corresponding to defect mode gets split and two peaks appear at λ =1560 &1600 nm as shown in Fig. 4.23. This resonance splitting phenomenon is a typical Fano resonance principle. Fano resonance is traditionally excited or observed in the region where the symmetry of the perfect photonic or plasmonic structure is marginally broken. But recently it is also reported that asymmetrical structure or symmetry breaking is not a necessary condition for Fano resonance. It will be observed in the region when there are an interplay between dark (sub-radiant) mode and bright (super-radiant) mode i.e. Fano resonance is excited as a result of destructive interference between radiative (bright) and non-radiative(dark) mode. The broad bright mode is the consequence of defect mode of grating which is directly excited through incoming signals while dark narrow mode is due to the presence of nano metallic slit. Bright modes are spectrally broad while dark modes are not radiative broad. The performance of filtering operation is quantified using Quality factor and FWHM (Full Width at Half Maximum). FWHM of 15 nm and Quality (Q-factor) approaching a value of 106 is obtained. The modification in the geometrical parameters lead to an enhanced value of Q-factor.

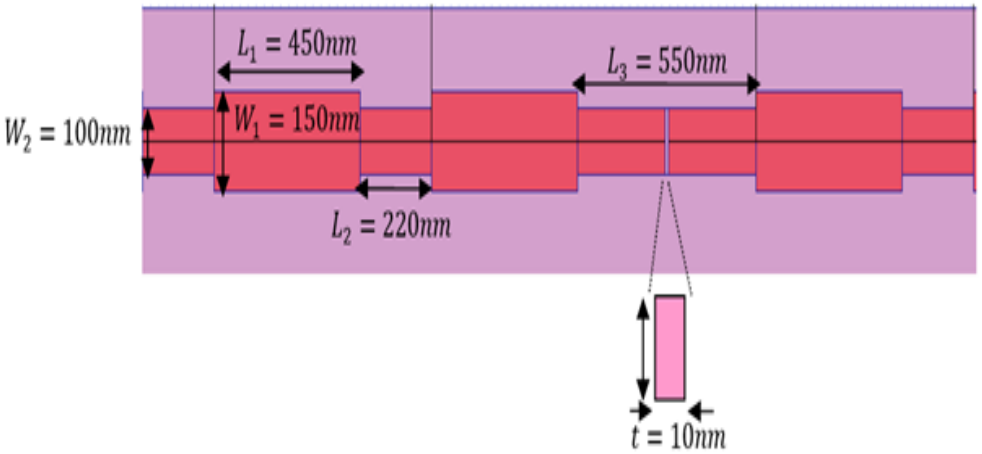

Figure 4.22: Plasmonic grating with defect length L_3 equal to 550 nm loaded with a metallic slit of width (t=10nm).

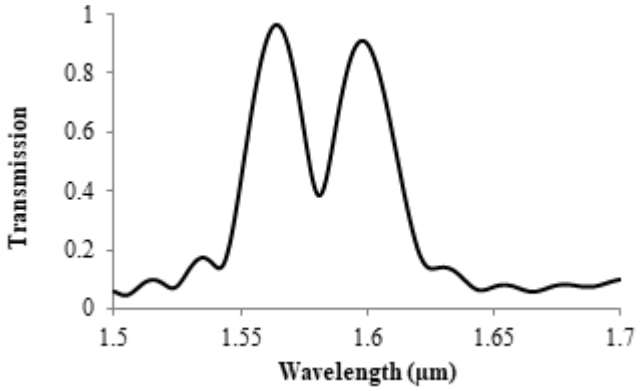

Figure 4.23: *Transmission spectrum of plasmonic grating loaded with metallic slit*

The excitation of the defect mode is through the input field. Thus it is called as highly radiative mode and it plays a vital role in exciting non-radiative mode. As the defect region is loaded with metallic slit, near field of slit modifies the surface plasmon resonance condition and the dark mode emerges in bright mode which splits the resonance into two peaks. The splitting between resonances can be stretched by shifting the location of the slit. Fig. 4.24 shows that resonance splitting increases with left and right shifting of metallic slit. By varying its thickness, dark mode frequency can be comfortably tuned. Tunable Fano resonance has wide applications in the areas of chemical and gas sensing, optical switches, slow light, buffers etc.

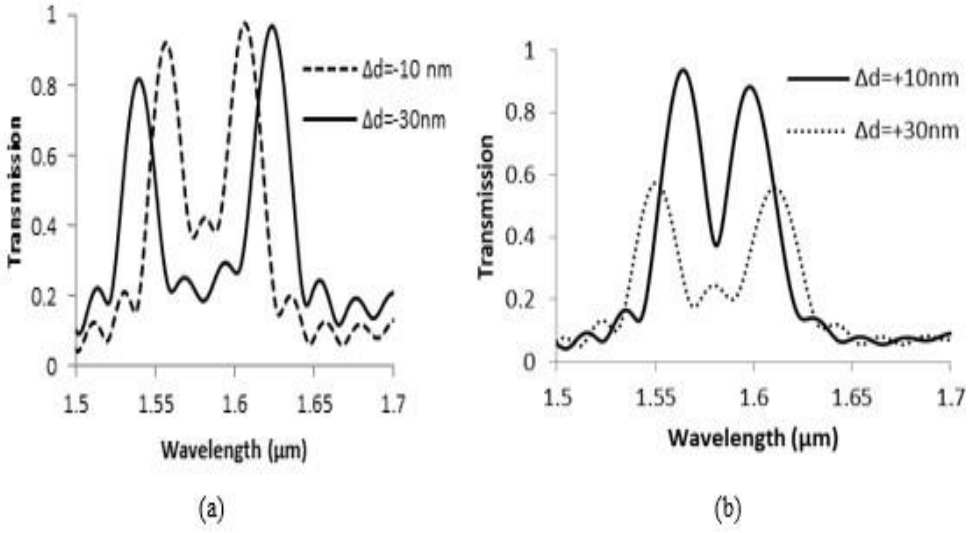

Figure 4.24: Transmission spectra with shifting of metallic slit to left and right from the centre of the defect as shown in (a) and (b) respectively.

4.6.1. Application in Switching

A dynamically tunable switch can also be realized using the proposed grating with nonlinear optical materials in defect region of grating. A nonlinear Kerr material is being used whose dielectric constant varies with pump intensity (electric field) according to given relation $\boldsymbol{\varepsilon = \varepsilon_0 + \chi^{(3)}|E^2|}$, where $\boldsymbol{\varepsilon_0}$ shows linear constant of dielectrivity, $\boldsymbol{\chi^{(3)}}$ is third order susceptibility and its value is $\boldsymbol{4.8 \times 10^{-10}\ esu}$. Pump light is inserted in the defect region. Fig. 4.25 shows the transmission spectrum under two different cases: in presence of pump light and in the absence of pump light. The spectrum is red shifted in the former case. Thus, the device which was presently at OFF state (in absence of pump light at λ=) is turned ON after applying pump light.

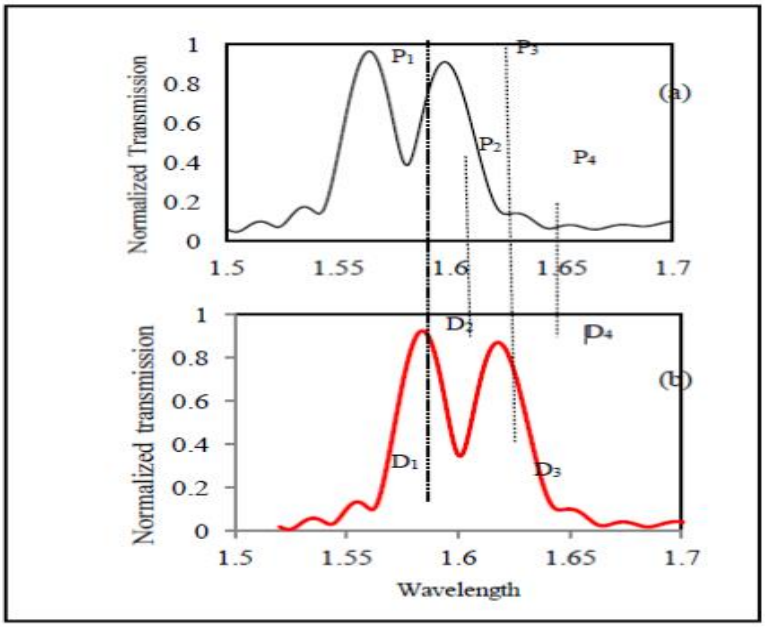

Figure 4.25: Spectrum of metallic slit coupled grating a) without pump signal b) with pump signal

Fig. 4.25 describes that multiple switching is observed at different wavelengths. The switching performance is analysed using modulation depth which is defined as: $\mathrm{M.D} = 10 \log \frac{\mathrm{T(I_{ON})}}{\mathrm{T(I_{OFF})}}$ [74,75] ; here $\mathrm{T(I_{ON})}$ is the transmission efficiency for ON state (presence of pump light) at λ= and $\mathrm{T(I_{OFF})}$ is efficiency for OFF state (absence of pump light) at the same wavelength. The proposed device offers a high value of modulation depth M.D.= Table 2 enlists ON and OFF transmission efficiency for different wavelengths. The highest M.D. is obtained at telecommunication wavelength. M.D. can be enhanced with increasing intensity of pump light.

Table 4.3: Multiple switching wavelength and related value of modulation depth

$\lambda\ (nm)$	T_{ON}	T_{OFF}	MD (dB)
1560	P_1=0.94	D_1=0.09	10.18
1578	D_2=0.89	P_2=0.4	3.4
1600	P_3=0.89	D_3=0.39	3.5
1620	D_4=0.875	P_4=0.12	8.6

Fig. 4.26 depicts variation in modulation depth against changing pump intensity. Thus, Fano resonance helps to design efficient plasmonic switch. As per this study, it can be claimed that the proposed structure reports better switching characteristics as compared to some previous work enlisted in Table 4.4.

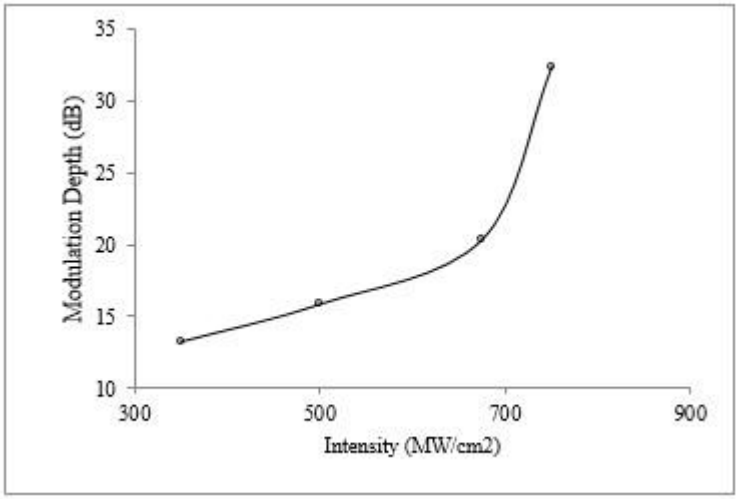

Figure 4.26: Variation of modulation depth for changing pump intensity

Table 4.4: Comparative study of the performance of the proposed switch with earlier stated work

References	M.D. (dB)
[75]	13.8 (T(on/off)=24)
[77]	6
[78]	18.3
[76]	30
[79]	30

4.7. Refractive index sensor

SPR technology is extensively used in optical refractive index sensing. As it enables on-chip integration of photonic circuits, researchers have taken a keen interest in the development of this technology and they have utilised it in several fields of food security [80], diagnosis [81], environmental monitoring [82]. Recently, nano-particles based on noble metals have been employed in optical sensing for augmenting the sensitivity because of their high sensitivity to change in refractive index (RI).

RI sensing is carried out by resonance condition monitoring at the detector. There are two techniques involved: angular interrogation and wavelength interrogation. In the angular interrogation method, the incident wavelength remains fixed, and the condition of resonance is observed (i.e. a sharp dip) at a particular angle of detection while in the other approach, detection angle is fixed and wavelength is varied to achieve condition of resonance [14]. These two parameters depend on the refractive index of the material. The resonance condition varies in accordance with the RI of the material under test. The traditional SPR sensing devices using prism coupling suffers from the drawback of large size and also the presence of movable parts. Moreover, in remote sensing applications, prism coupled SPR sensors cannot be used.

Localized Surface Plasmons (LSPs) and Surface Plasmon Polariton (SPPs) based resonances are extensively employed in the designing of label-free refractive index sensors characterizing large sensitivity and confining the light way beyond diffraction limit [11]. The propagating SPs enable the propagation of plasmons along the metal-insulator interface, whereas LSPs produce the local oscillations of plasmons in the nano structures. The evanescent field has a decay length of the order of 100's of nm in SPs and just few nm in LSPs. This very short decay length helps in improving the sensitivity to any change in surface RI.

Both the resonances exhibit fascinating characteristics and unique advantages to be used in sensing applications. Sensors based on LSPRs are very simple and cheap for sensing a change in RI due to the adsorption of target molecules. The generation of localized plasmons leads to broad peak of resonance which in turn curtails the FOM of LSPR sensors. From the broad resonance spectrum Q-factor obtained is small and it also results in surge of radiation losses. The practical utility of the sensors is limited by huge radiation losses. Therefore, SPR based sensors are better for gaining high sensitivity as well as enhanced FOM [24].

4.7.1. Performance Analysis

To employ the plasmonic grating as a RI sensor, initially air is filled in the defect region and then in the steps of 0.1 the refractive index is increased. Fig. 4.27 shows that the transmission spectra get red shifted and with the increase in refractive index of defect region the defect mode is observed for longer wavelengths as depicted in Fig. 4.28.

The performance of the device is quantified using two parameters: Sensitivity and FOM. Sensitivity (S) is defined as the change in wavelength per unit refractive index (RIU).

$$S = \frac{\Delta\lambda}{\Delta n}$$

Where $\Delta\lambda$ and Δn denote wavelength change and refractive index change respectively. From the FDTD simulations it can be seen that in the absence of metallic slit in the defect area, for 0.1 change RIU, the shift in wavelength is around 30.6 nm whereas in the presence of slit in the defect region the shift in wavelength is approximately 30.3 nm. Therefore, we can conclude that the sensitivities for the former and later cases are 306 nm/RIU and 303 nm/RIU respectively.

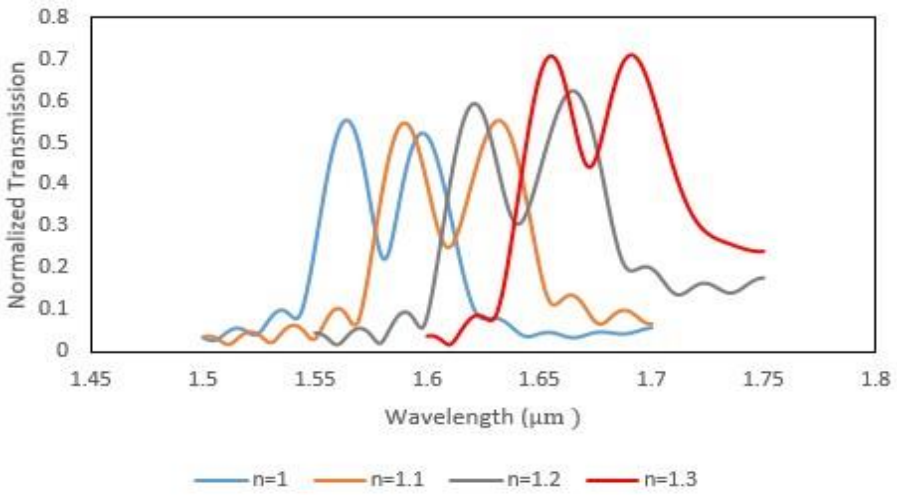

Figure 4.27: Transmission spectra as a function of refractive index

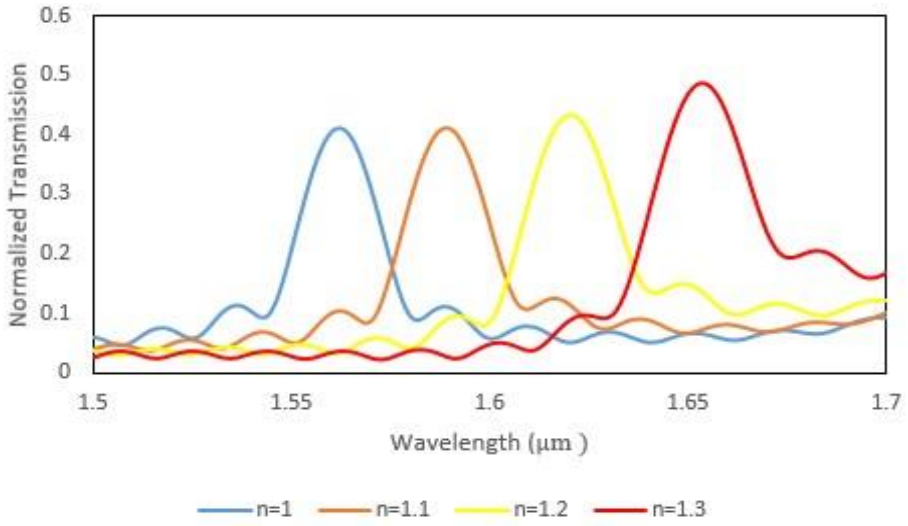

Figure 4.28: *Transmission spectra as a function of refractive index of the defect region*

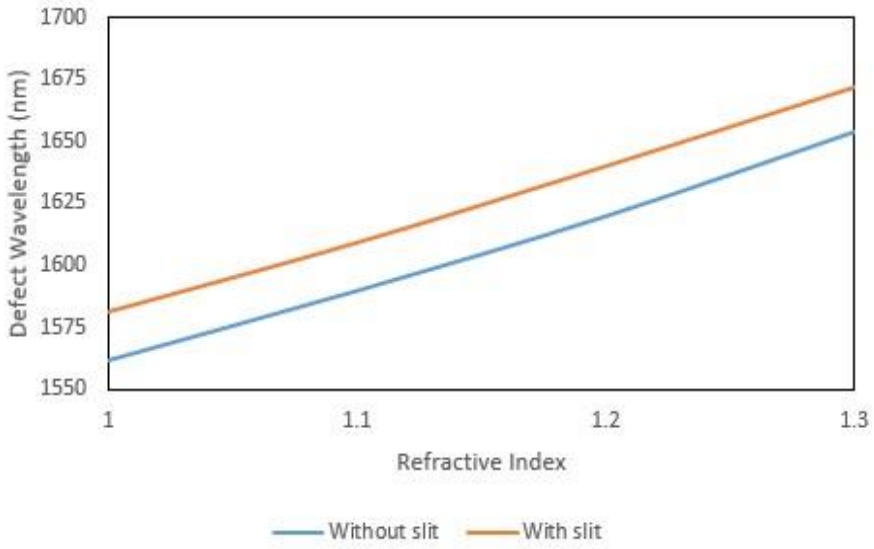

Figure 4.29: Variation of the defect wavelength

Fig 4.29 shows that with the increasing refractive index the defect wavelength gets shifted to higher values.

5. CONCLUSIONS AND FUTURE PROSPECTS

5.1. Thesis Conclusion

In this dissertation work, numerical analysis of MIM based Plasmonic grating has been investigated. MIM waveguide supports a unique feature of deep sub-wavelength confinement and it can confine signals far beyond the diffraction limit. The applications of the Plasmonic grating is explored in the fields of band stop filtering, refractive index sensing and multiple switching.

Several configurations of the MIM waveguide have been investigated for obtaining better filtering characteristics and enhanced stop bands have been obtained. The Quality Factor of the grating is significantly improved by tuning the geometrical parameters which makes the device suitable for the designing of different optical components, couplers, refractive index sensors etc. The MIM grating has facilitated an asymmetric line shaped Fano resonance. An all optical switch is designed by exciting Fano resonance in the waveguide. The switch operates in near-infrared region and can perform multiple switching at four different wavelengths. The performance of the device is quantified using modulation depth and quality factor. The improvement in modulation depth is also studied for increasing pump intensity.

5.2. Future prospects

The proposed work can find its suitability in controlling non-linearity by changing the gap. By tailoring a single geometrical parameter i.e. nanoslit, non-linear phenomenon can be further enhanced. These non-linear systems may be possible for different applications like SERS, biosensing etc. Furthermore, the proposed device can also be modified for demultiplexing application which is quite useful in telecommunications. By selecting proper geometrical parameters, a dense WDM system can be generated.

BIBLIOGRAPHY

[1] Chris A. Mack, "Fifty Years of Moore's Law," IEEE Transactions on Semiconductor Manufacturing, Vol. 24, No. 2, May 2011, (pp. 202 - 207).

[2] Ekmel Ozbay, "Plasmonics: Merging Photonics and Electronics at Nanoscale Dimensions," Science, Vol. 311, January 2006, (pp. 189-193).

[3] Karl Rupp, and Siegfried Selberherr, "The Economic Limit to Moore's Law" IEEE Transactions on Semiconductor Manufacturing, Vol. 24, No. 1, February 2011, (pp 1 - 4).

[4] J.D. Joannopoulus, Pierre R. Villeneuve & Shanhui Fan, "Photonic crystals: Putting a New Twist on Light," Nature, Vol 386, March 1997, (pp. 143 – 149).

[5] C. Jamois, R.B. Wehrspohn, L.C. Andreani, C. Hermann, O. Hess, U. Gosele, "Silicon-based Two-Dimensional Photonic Crystal Waveguides," Elsevier-Photonics and Nanostructures – Fundamentals and Applications 1, 2003. (pp. 1–13)

[6] Hamza Kurt, "Bend-Free Optical Power Transfer using Photonic Crystal Waveguide Arrays" IEEE Journal of Lightwave Technology, Vol. 27, No. 10, May 15, 2009, (pp. 1402 – 1407)

[7] Wei Wang, Bo Yang, "Characteristics Analysis of Photonic Crystal fiber with Rhombus Air-Core" Elsevier-Optik, Vol. 123, Issue 18, September 2012 (pp. 1669–1672)

[8] Rakhi Bhattacharya, S. Konar, "Extremely large birefringence and shifting of zero dispersion wavelength of photonic crystal fibers, " Elsevier-Optics & Laser Technology Volume 44, Issue 7, October 2012 (pp. 2210–2216).

[9] Fu-Li Hsiao and Chengkuo Lee, "Novel Biosensor Based on Photonic Crystal Nano-Ring Resonator, " Proceedings of the Eurosensors XXIII conference Procedia Chemistry Volume 1, Issue 1, September 2009 (pp. 417-420)

[10] Reed, Graham T. Silicon Photonics: The State of the Art. Chichester: Wiley, 2008. (ISBN: 978-0-470-02579-6)

[11] Stefan A. Maier, "Plasmonics: The Promise of Highly Integrated Optical Devices, "IEEE Journal Of Selected Topics In Quantum Electronics, Vol. 12, No. 6, November/December 2006 (pp. 1671-1677)

[12] Rashid Zia, Jon A. Schuller, Anu Chandran, and Mark L. Brongersma, "Plasmonics:The Next Chip-Scale Technology," Materials Today, Vol. 9, No. 7-8, July-August2006, (pp. 20–27).

[13] Xiaopeng Shen, Tie Jun Cui, Diego Martin-Cano, and Francisco J. Garcia-Vidal,"Conformal Surface Plasmons Propagating on Ultrathin and Flexible Films, " PNAS vol. 110, no. 1, January 2, 2013, (pp. 40–45).

[14] Stefan A. Maier, "Plasmonics: Fundamentals And Applications," Springer 2007(ISBN: 978-0-387-37825-1)

[15] Maria Makarova, Yiyang Gong, Szu-Lin Cheng, Yoshio Nishi, Selcuk Yerci, Rui Li, Luca Dal Negro, and Jelena Vuckovic, "Photonic Crystal and Plasmonic Siliconbased Light Sources" IEEE Journal of Selected Topics in Quantum Electronics, Vol.16, No. 1, January/February 2010, (pp. 132 - 140)

[16] Zhanghua Han and Sergey I Bozhevolnyi, "Radiation Guiding with Surface Plasmon Polaritons" IOP Publishing, Rep. Prog. Phys. Volume 76, Number 1, 2013, (page.016402)

[17] Chen, Y., Yu, Y., Li, X., Zhou, H., Hong, X. and Geng, Y., 2016. Fiber-optic urine specific gravity sensor based on surface plasmon resonance. *Sensors and Actuators B: Chemical*, *226*, pp.412-418.

[18] Emmanouil-Panagiotis Fitrakis, Thomas Kamalakis, and Thomas Sphicopoulos,"Slow Light in Insulator–Metal–Insulator Plasmonic Waveguides" Journal of the Optical Society of America B, Vol. 28, Issue 9, 2011, (pp. 2159-2164).

[19] Lu, Hua, Xueming Liu, Leiran Wang, Yongkang Gong, and Dong Mao. "Ultrafast all-optical switching in nanoplasmonic waveguide with Kerr nonlinear resonator." *Optics express* 19, no. 4 (2011): 2910-2915.

[20] Xie, Yi-Yuan, Chao He, Jia-Chao Li, Ting-Ting Song, Zhen-Dong Zhang, and Qian-Ren Mao. "Theoretical investigation of a plasmonic demultiplexer in MIM waveguide crossing with multiple side-coupled hexagonal resonators." *IEEE Photonics Journal* 8, no. 5 (2016): 1-12.

[21] Nurmohammadi, T., Abbasian, K. and Yadipour, R., 2017. A proposal for a demultiplexer based on plasmonic metal–insulator–metal waveguide-coupled ring resonator operating in near-infrared spectrum. *Optik*, *142*, pp.550-556.

[22] Boxun Li, Hongjian Li, Lili Zeng, and Hui Yang, "Tunable Filter and Optical Buffer based on Dual Plasmonic Ring Resonators" Taylor & Francis, Journal of Modern Optics, Vol. 62 , Issue 3, February 2015, (pp. 186-194).

[23] Wang, W., Mai, Z., Chen, Y., Wang, J., Li, L., Su, Q., Li, X. and Hong, X., 2017. A label-free fiber optic SPR biosensor for specific detection of C-reactive protein. *Scientific reports*, *7*(1), p.16904.

[24] Zafar, Rukhsar, and Mohammad Salim. "Enhanced figure of merit in Fano resonance-based plasmonic refractive index sensor." *IEEE Sensors Journal* 15, no. 11 (2015): 6313-6317.

[25] Han, Z., Forsberg, E. and He, S., 2007. Surface plasmon Bragg gratings formed in metal-insulator-metal waveguides. *IEEE Photonics Technology Letters*, *19*(2), pp.91-93.

[26] Hu, F., Yi, H. and Zhou, Z., 2011. Band-pass plasmonic slot filter with band selection and spectrally splitting capabilities. *Optics Express*, *19*(6), pp.4848-4855

[27] Zheng, G., Chen, Y., Xu, L., Lai, M. and Liu, Y., 2013. Metal–insulator–metal waveguide-based band-pass filter with circular ring resonator containing Kerr nonlinear medium. *Optics Communications*, *305*, pp.164-169.

[28] Chen, X., Lang, P., Liu, G., Zhang, R. and Zhong, T., 2013. Surface plasmon polariton based band-pass and stop-band filters in symmetric double ring resonators. *Journal of Modern Optics*, *60*(21), pp.1910-1914.

[29] Zafar, R. and Salim, M., 2015. Enhanced figure of merit in Fano resonance-based plasmonic refractive index sensor. *IEEE Sensors Journal*, *15*(11), pp.6313-6317.

[30] Yan, S.B., Luo, L., Xue, C.Y. and Zhang, Z.D., 2015. A refractive index sensor based on a metal-insulator-metal waveguide-coupled ring resonator. *Sensors*, *15*(11), pp.29183-29191.

[31] Zafar, R. and Salim, M., 2016. Enhanced phase sensitivity in plasmonic refractive index sensor based on slow light. *IEEE Photonics Technology Letters*, *28*(20), pp.2187-2190.

[32] Qu, S., Song, C., Xia, X., Liang, X., Tang, B., Hu, Z.D. and Wang, J., 2016. Detuned plasmonic Bragg grating sensor based on a defect metal-insulator-metal waveguide. *Sensors*, *16*(6), p.784.

[33] Wei, Z., Li, X., Yin, J., Huang, R., Liu, Y., Wang, W., Liu, H., Meng, H. and Liang, R., 2016. Active plasmonic band-stop filters based on graphene metamaterial at THz wavelengths. *Optics express*, *24*(13), pp.14344-14351

[34] Luo, X., Zhai, X., Wang, L., Lin, Q. and Liu, J., 2017. Theoretical analysis of plasmon-induced transparency in MIM waveguide Bragg grating coupled with a single subradiant resonator. *IEEE Photonics Journal*, *9*(5), pp.1-8.

[35] Zafar, R., Nawaz, S., Singh, G., d'Alessandro, A. and Salim, M., 2018. Plasmonics-based refractive index sensor for detection of hemoglobin concentration. *IEEE Sensors Journal*, *18*(11), pp.4372-4377.

[36] Iqbal, T., Khalil, S., Ijaz, M., Riaz, K.N., Khan, M.I., Shakil, M., Nabi, A.G., Javaid, M., Abrar, M. and Afsheen, S., 2019. Optimization of 1D plasmonic grating of nanostructured devices for the investigation of plasmonic bandgap. *Plasmonics*, *14*(3), pp.775-783.

[37] http://mqm.aast.edu/staffcourses/66_12485_EC311_2013_1__1_1_Chapter_6_Free_electron_in_solids.pdf

[38] Sergey I Bozhevolnyi, "Plasmonic Nanoguides and Circuits" Pan Stanford Publishing Pte. Ltd. Copyright 2009 (ISBN-13 978-981-4241-32-8)

[39] ITMO University (2019). Plasmonics: From Fundamentals to Modern Applications. Available:https://www.edx.org/course/plasmonics-from-fundamentals-to-modern-applications

[40] Ian Freestone, Nigel Meeks, Margaret Sax and Catherine Higgitt, "The Lycurgus Cup: A Roman Nanotechnology" Gold Bulletin, Vol. 40, Issue 4, December 2007, (pp. 270–277).

[41] M. Faraday, "The Bakerian Lecture: Experimental Relations of Gold (and Other Metals) to Light" Philosophical Transactions of the Royal Society of London 147,1857, (pp. 145-181).

[42] Where now for plasmonics?, Nature Nanotechnology Vol. 11, No. 1, January (2016). (doi:10.1038/nnano.2015.333).

[43] R.Ortuno, C. Garcıa-Meca, F. J. Rodrıguez-Fortuno, and A. Martınez,"Extraordinary Transmission and Light Confinement in Subwavelength Metallic Films Apertures," Progress in Electromagnetics Research Symposium Proceedings,Vol. 7, No. 5, 2011, (pp.471-475)

[44] Chris D. Geddes, "Reviews in Plasmonics 2010" Springer, ©2012. (ISBN 978-3-319-48080-0)

[45] Alongkorn Pimpin and Werayut Srituravanich "Review on Micro-andNanolithography Techniques and their Applications" Engineering Journal Vol. 16 Issue 1, Jan 2012, (pp. 37-56).

[46] R.Zafar, "Investigation of Optical Buffering and Refractive Index Sensing characteristcis in Fano resonance-based metal-insulator-metal Plasmonic waveguide" Ph.D. dissertation, Dept. ECE, MNIT, Jaipur, India,2016

[47] Sophocles J. Orfanidis, "Electromagnetic Waves and Antennas," Rutgers UniversityCopyright © 1999–2016.

[48] Ziyuan Li, Haroldo T. Hattori, Lan Fu, Hark Hoe Tan, and Chennupati Jagadish,"Merging Photonic Wire Lasers and Nanoantennas" IEEE-Journal of LightwaveTechnology, Vol. 29, No. 18, September 15, 2011, (pp. 2690 - 2697)

[49] Jennifer A. Dionne, Ewold Verhagen, Albert Polman, and Harry A. Atwater, "Are Negative Index Materials Achievable with Surface Plasmon Waveguides? A CaseStudy of Three Plasmonic Geometries," OSA publishing, Opt. Exp., Vol. 16, No. 23, November 2008, (pp. :19001-19017.).

[50] Pierre Berini, "Long-range surface plasmon polaritons," Advances in Optics and Photonics, Vol. 1, Issue 3, 2009, (pp. 484-588)

[51] Alexei A. Maradudin, J. Roy Sambles, and William L. Barnes, "Modern Plasmonics" Elsevier Handbook of Surface Science, Vol. 4, 2014 (ISBN 978-0444-59526-3)

[52] Jianlong Liu, Guangyu Fang, Haifa Zhao,Yan Zhang, Shutian Liu, "Surface Plasmon Reflector based on Serial Stub Structure" OSA publishing, Optics Express Vol. 17, No. 22, October 2009, (page no. 20134-20139).

[53] Yong S Joe, Arkady M Satanin and Chang Sub Kim, "Classical analogy of Fano resonances" IOP Science Phys. Scr. 74, 2006, (pp. 259–266)

[54] B. Gallinet, A. Lovera, T. Siegfried, H. Sigg and O.J.F. Martin, "Fano Resonant Plasmonic Systems: Functioning Principles and Applications," The Fifth International Workshop on Theoretical and Computational Nano-Photonics, AIP Conf. Proc. Volume 1475, Issue 1, 2012, (pp. 18-20). (doi:10.1063/1.4750081)

[55] Xianji Piao, Sunkyu Yu, Sukmo Koo, Kwanghee Lee, and Namkyoo Park, "Fano-Type Spectral Asymmetry and its Control for Plasmonic Metal-Insulator-Metal Stub Structures," OSA Publishing, Optics Express, Vol. 19, No. 11, 2011, (pp. 10907- 10912).

[56] M. Galli, S. L. Portalupi, M. Belotti, L. C. Andreani, L. O'Faolain, and T. F. Krauss, "Light scattering and Fano resonances in High-Q Photonic Crystal Nanocavities," Applied Physics Letters 94, 2009, (Page no. 071101)

[57] Ranjan Singh, Ibraheem Al-Naib, Wei Cao, "The Fano Resonance in Symmetry Broken Terahertz Metamaterials", IEEE Transactions on Terahertz Science and Technology, Vol. 3, No. 6, November 2013, (pp. 820 – 826).

[58] Xianji Piao, Sunkyu Yu, Sukmo Koo, Kwanghee Lee, and Namkyoo Park, "Fano-Type Spectral Asymmetry and its Control for Plasmonic Metal-Insulator-Metal Stub Structures," OSA Publishing, Optics Express, Vol. 19, No. 11, 2011, (pp. 10907-10912).

[59] J. B. Lassiter, H. Sobhani, J. A. Fan, J. Kundu, F. Capasso, P. Nordlander, and N. J.Halas, "Fano Resonances in Plasmonic Nanoclusters: Geometrical and Chemical Tunability," Nano Lett. 10(8), 2010, (pp: 3184–3189).

[60] R. Wood, "On the Remarkable Case of Uneven Distribution of Light in a Diffraction Grating Spectrum," Proc. R. Soc. London, Ser. A 18, 1902, (pp: 269–275).

[61] Wood, R. W., "Anomalous Diffraction Gratings," Phys. Rev. 48, 1935, (pp. 928–936).

[62] L. Rayleigh, "On the Dynamical Theory of Gratings," Proc. R. Soc. London, Ser. A 79, 1907, (pp. 399–416).

[63] U. Fano, "Some Theoretical Considerations on Anomalous Diffraction Gratings," Phys. Rev. 50, 573, 1936, (page no. 573).

[64] U. Fano, "On the Anomalous Diffraction Gratings. II," Phys. Rev. 51, 288, 1937,(page no. 288).

[65] U. Fano, "The Theory of Anomalous Diffraction Gratings and of Quasi-stationary Waves on Metallic Surfaces Sommerfield's Waves," J. Opt. Soc. Am. 31, 1941(pp: 213–222).

[66] Reza Asadi, Mohammad Malek-Mohammad, Sina KhorasanI, "All-Optical Switch Based on Fano Resonance in Metal Nanocomposite Photonic Crystals" Optics Communications, Vol. 284, Issue 8, April 2011, (pp. 2230–2235).

[67] Kunhua Wen, Lianshan Yan, Wei Pan, Member, Bin Luo, Member, Zhen Guo,Yinghui Guo, and Xiangang Luo, "Electromagnetically Induced Transparency-LikeTransmission in a Compact Side-Coupled T-Shaped Resonator" IEEE Journal of Lightwave Technology, Vol. 32, No. 9, May, 2014, (pp. 1701-1707)

[68] Yanik AA, Cetin AE, Huang M, Artar A, Mousavi SH, Khanikaev A, Connor JH,Shvets G, and Altug H, "Seeing Protein Monolayers with Naked Eye throughPlasmonic Fano Resonances" Proc Natl Acad Sci U S A. 108(29), Jul, 2011, (pp.11784–11789)

[69] Y. Francescato, V. Giannini, and S. A. Maier, "Plasmonic Systems Unveiled by Fano Resonances," ACS Nano 6(2), 2012, (pp. 1830–1838).

[70] Xianji Piao, Sunkyu Yu, and Namkyoo Park, "Control of Fano Asymmetry in Plasmon Induced Transparency and its Application to Plasmonic Waveguide Modulator," OSA Publishing, Optics Express, Vol. 20, No. 17, 2012, (pp. 18994-18999).

[71] H. Lu, X. Liu, D. Mao, and G. Wang, "Plasmonic Nanosensor based on FanoResonance in Waveguide-Coupled Resonators," Opt. Lett. 37(18), 2012 (pp.: 3780–3782).

[72] Z. Yang, Q. Wu, and H. Lin, "Tunable Two Types of Fano Resonances in Metal-Dielectric Core-Shell Nanoparticle Clusters," Appl. Phys. Lett. 103(11), 2013.(doi: http://dx.doi.org/10.1063/1.4821187)

[73] H.C. Guo, N. Liu, L.W. Fu, T.P. Meyrath, T. Zentgraf, H. Schweizer, and H.Giessen, Resonance Hybridization in Double Split-Ring Resonator Metamaterials, OSA Publishing, Opt. Express 15 (19), 2007 (pp.: 012095–12101).

[74] He, Z., Li, H., Zhan, S., Li, B., Chen, Z. and Xu, H., 2015. Tunable multi-switching in plasmonic waveguide with Kerr nonlinear resonator. *Scientific reports*, *5*, p.15837.

[75] Nurmohammadi, T., Abbasian, K. and Yadipour, R., 2018. Ultra-fast all-optical plasmonic switching in near infra-red spectrum using a Kerr nonlinear ring resonator. *Optics Communications*, *410*, pp.142-147.

[76] Chen, Z., Song, X., Duan, G., Wang, L. and Yu, L., 2015. Multiple Fano resonances control in MIM side-coupled cavities systems. *IEEE Photonics Journal*, *7*(3), pp.1-10.

[77] Ahadi, S., and N. Granpayeh. "Kerr nonlinear all-optical switches based on asymmetric plasmonic T-shaped single slit." In 2015 23rd Iranian Conference on Electrical Engineering, pp. 343-347. IEEE, 2015.

[78] Li, Jian, Jin Tao, Zan Hui Chen, and Xu Guang Huang. "All-optical controlling based on nonlinear graphene plasmonic waveguides." Optics express 24, no. 19 (2016): 22169-22176.

[79] Kong, Yan, Rong Lin, Wenchao Qian, Qi Wei, Cheng Liu, and Shouyu Wang. "Active dual-wavelength optical switch-based plasmonic demultiplexer using metal-Kerr nonlinear material-metal waveguide." IEEE Photonics Journal 9, no. 4 (2017): 1-8.

[80] F. S. Ligler, C. R. Taitt, L.C. Shriver-Lake, K.E. Sapsford, Y. Shubin, and J.P. Golden, “Array Biosensor For Detection Of Toxins” Anal. Bioanal. Chem. 377(3), 2003, (pp: 469-477).

[81] Yonzon, C.R., Haynes, C.L., Zhang, X., Walsh, J.T. and Van Duyne, R.P., 2004. A glucose biosensor based on surface-enhanced Raman scattering: improved partition layer, temporal stability, reversibility, and resistance to serum protein interference. *Analytical Chemistry*, *76*(1), pp.78-85.

[82] J Ji, A Schanzle, & MB Tabacco, “Real-Time Detection of Bacterial Contamination in Dynamic Aqueous Environments using Optical Sensors. Anal Chem. 76, 2004 (pp: 1411–1418).

Thesis

ORIGINALITY REPORT

5%	0%	1%	5%
SIMILARITY INDEX	INTERNET SOURCES	PUBLICATIONS	STUDENT PAPERS

PRIMARY SOURCES

1	Submitted to Malaviya National Institute of Technology Student Paper	4%
2	Han, Song, Ranjan Singh, Longqing Cong, and Helin Yang. "Engineering the fano resonance and electromagnetically induced transparency in near-field coupled bright and dark metamaterial", Journal of Physics D Applied Physics, 2015. Publication	<1%
3	Submitted to University of Babylon Student Paper	<1%
4	icnp.rcas.sinica.edu.tw Internet Source	<1%
5	Hermann A. Haus. "Electromagnetic Noise and Quantum Optical Measurements", Springer Nature, 2000 Publication	<1%
6	Jin, . "Transmission Lines and Plane Waves", Theory and Computation of Electromagnetic	<1%